STABILITY AND FUNCTIONAL STUDIES OF OLIGOMERIC M2 ION CHANNELS IN SYNTHETIC AND NATURAL LIPID ENVIRONMENTS

By

FRANK JOSEPH RAUCCI

A THESIS PRESENTED TO THE GRADUATE SCHOOL
OF THE UNIVERSITY OF FLORIDA IN PARTIAL FULFILLMENT
OF THE REQUIREMENTS FOR THE DEGREE OF MASTER OF SCIENCE

UNIVERSITY OF FLORIDA

2004

ACKNOWLEDGEMENTS

First, I would like to thank my committee members, Joanna Long, Arthur Edison, and Thomas DeMarse for their guidance, advice, and support. I would also like to thank Randolf Duran and Peter Anderson for their advice during the course of this project. Their help was invaluable. Next, I would like to thank all the students and post-doctoral members of the groups involved in this project for their help in data acquisition and analysis. This work could not have been completed without the help of Kun Fang, Jun Zhang, Frank Mills, Chris Williams, Brian Dorvel, Joy Wattawa, and Becky Price. I would also like to thank my parents for their love and support. I would like to thank my friends for their understanding during some long nights and I would like to specifically thank Jennifer Cullem and Kaveri Marathe. And last but certainly not least, I would like to thank my fiancée, Kalyani Marathe, for her love and understanding during this very hectic time. I could not have completed this work without her.

TABLE OF CONTENTS

LIST OF TABLES

LIST OF FIGURES

Abstract of Thesis Presented to the Graduate School
of the University of Florida in Partial Fulfillment of the
Requirements for the Degree of Master of Science

STABILITY AND FUNCTIONAL STUDIES OF OLIGOMERIC M2 ION CHANNELS IN SYNTHETIC AND NATURAL LIPID ENVIRONMENTS

By

Frank Joseph Raucci

December 2004

Chair: Thomas DeMarse
Major Department: Biomedical Engineering

The self-assembly properties of the ion channel-forming peptide segment of the nicotinic acetylcholine receptor, M2, were examined at the air-water interface. The properties of monolayers formed by the peptide alone were compared to mixtures of M2 with a synthetic lipid, 1,2-diphyanoyl-*sn*-glycero-3-phosphocholine (DPhPC) and the lipid and peptide alone via Langmuir-Blodgett surface pressure-area isotherms and Brewster Angle Microscopy. The DPhPC monolayer remains in a single phase until its collapse pressure whereas the M2 monolayer undergoes two distinct phase transitions before collapse. M2 ion channel fluctuations were studies via tip-dipped patch clamp methodologies with DPhPC and native lipid environments. Single channel fluctuations were recorded and evaluated to determine the stochastic response of the ion channel to applied voltages. The results show that the M2 ion channel is voltage gated and relatively stable. The pertinence of these results to characterizing the stability and function of this ion channel in synthetic membranes will be discussed.

CHAPTER 1
INTRODUCTION

Project Overview

The immediate goal of this project is to study the effects of lipid environment on the properties of a synthetic ion channel incorporated into a lipid bilayer. This goal encompasses achieving lipid bilayer membrane resistances greater than 10^6 Ω cm^2, quantifying channel opening response times, and measuring single-channel current fluctuations at low channel concentrations. The selected ion channel is the pore-forming M2 δ-subunit of the nicotinic acetylcholine receptor, which is present in many biologically relevant systems.

The ultimate goal of this project is to use surface immobilization and encapsulation within polymer-modified, tethered lipid bilayers in order to engineer thin films of oriented, addressable, ion channels. The channels would then be used as small biosensors that could detect minute amounts of a particular agonist in aqueous solution. Possible microelectronic detection methods for channel function might include ion-sensitive microelectrode arrays (MEA's), field effect transistors (FET's), or microelectrodes as extended gates of FET's.

The fundamental principles governinig ion channel behavior in synthetic membranes elucidated from our studies could be extended beyond the initial ion channel being characterized in this work and may thus be applied to a variety of biosensors incorporating biological and synthetic ion channels with myriad functions, physiological or otherwise. The possibility of improved medical diagnostics for a number of toxicity-causing agents that affect the ion flow across cellular membranes in humans may be realized by integrating the ion channels with electronics. Applications are also apparent in agricultural and military settings, as both would benefit from

a valuable diagnostic that could offer rapid detection of excessive acetylcholine concentrations at the nicotinic-acetylcholine receptor caused by organo-phosphate exposure or other agonist interactions. Also, such a device could possible be extended as a potent alternative to tissue harvest or human and animal research in areas such as pharmacology. The potential for rapid throughput assays of the effect of new chemical entities on ion channels also exists for functional biosensors.

As the nicotinic acetylcholine receptor is present in many tissue types, including neurons and muscle, understanding how the channel mechanism is affected by the surrounding lipid environment could also have a more direct medical impact. Nicotine and several anesthetics are numbered among the known agonists and antagonists of nAChR which makes this protein an attractive model for studying signal transduction.

Ion Channels

Ion channels play an integral role in many biological functions, including nerve and muscle activity (Hucho and Wiese, 2001). Virtually all membranes in living cells display a separation of potential across them due **to** an unequal distribution of ions in the intracellular and extracellular domains. This charge separation creates voltage which is termed membrane potential. These potential differences play important yet distinct roles in different biological cells. For instance, nerve cells use depolarization signals called action potentials that travel the length of the nerve axons to communicate with other nerve cells at synaptic junctions. The value of the potential difference across the lipid membranes of any cell is given by the Goldman-Hodgkin-Katz Equation, which is a derivation of the Nernst equation. This equation depends on the relative permeabilities, P_X, and the internal, $[X]_i$, and external, $[X]_e$, concentrations of the respective ions present as well as the temperature and the gas constant, R, and the Faraday constant, F (Hille, 2001). Note that unlike the Nernst equation, the zero-current

potential in this case is in fact non-zero and represents a steady-state movement of ions away from equilibrium.

$$E = \frac{RT}{F} \ln \frac{P_{Na}[Na^+]_e + P_K[K^+]_e + P_{Cl}[Cl^-]_i}{P_{Na}[Na^+]_i + P_K[K^+]_i + P_{Cl}[Cl^-]_e}$$

The lipid bilayers of plasma membranes provide a significant energy barrier to the movement of charged particles from the intracellular to extracellular domains and vice versa, thus allowing for the establishment of these membrane potentials. In order to transport ions between the two ionic reservoirs on either side of the plasma membrane, the cells make use of specialized, gated transmembrane proteins, known as ion channels, to facilitate the ion currents.

Ion channels have many distinct features that make them of interest for biophysical and physiological study. The first characteristic property of ion channels is their high ion selectivity. Channels not only show selectivity between anionic or cationic molecules but also between monovalent and divalent ions or even for a specific ion, such as H^+(Hille, 2001). Secondly, ions channels are dynamic proteins, which demonstrate identifiable responses under specified conditions. At resting potential, the channels are completely closed and impermeable to ion current flow. However, they can be opened, or gated, by either a change in the membrane potential or the binding of particular ligands (Hucho and Weise, 2001). Thus the two important functional components characteristic of all ion channels are a selectivity filter that determines which ions will be allowed to pass through the channel pore and a gating mechanism that controls the opening of the pore. The two major classes of ion channels are described by their gating mechanisms and thus all channels can be classified as either voltage-gated or ligand-gated. Ligand-gated channels undergo a conformational change when a particular agonist binds to a receptor site. Voltage-gated channels usually undergo a conformational change within the lipid membrane due to

a particular, usually polar segment, of the structure orienting within the electric field between the two lipid layers of the membrane bilayer (Hille, 2001).

Nicotinic Acetylcholine Receptors

Channels are further classified into families and superfamilies based on functional and sequential characteristics. There are three superfamilies of ligand-gated channels: the ATP-gated purino receptors, the ionotropic glutamate receptors, and receptors that are similar to the nicotinic acetylcholine receptor (Hille, 2001). The last superfamily, which will be our primary focus, includes the nicotinic acetylcholine receptor (nAChR), as well as glycine receptors, $GABA_A$ receptors, and some serotonin receptors (Hucho and Weise, 2001). These constituents have similar sequences and many conserved structural features. They all share similar glycosylation patterns, comparable peptide loops created by disulfide bridges, similar distributions of prolines, and conserved serine and threonine polar residues in the channel-forming domain (Hucho and Weise, 2001). The most important feature shared by all of the receptors in this superfamily is the presence of four hydrophobic amino acid sequences that span the plasma membrane, labeled M1 through M4.

The pore of the nicotinic acetylcholine receptor (nAChR) was the first channel pore to be characterized using mutagenesis. These studies identified the residues of the pore-lining segments and also characterized the selectivity filter function of the channel was described. The functional form of nAChR is composed of five homologous subunit proteins which each have the four hydrophobic, transmembrane segments (M1-M4) that are characteristic of their superfamily. The nAChR is found in many cells, including those responsible for signaling in neuronal and muscular tissues, and can be composed of slightly different homologues. The stoichiometry of the nAChR varies significantly depending on where the channel is found. In muscule tissue, nAChR has a composition of $\alpha_2 \cdot \beta \cdot \gamma \cdot \delta$ while neuronal nAChR is a homopentamer composed of α subunits (Oblatt-Montal *et al.*, 1993). As its name implies, the nAChR is a ligand-gated

channel that responds to the neurotransmitting agonist acetylcholine *in vivo*, while also demonstrating response to other agonists such as nicotine (Hucho and Weise, 2001). In the full receptor, the agonist binding sites are located between the two α subunits and between the α subunit and the adjacent γ and δ subunits in the $\alpha_2 \cdot \beta \cdot \gamma \cdot \delta$ form of nAChR (Hille, 2001).

The self-assembled pentamers form a central pore which has an effective pore diameter of less than or equal to 7 Å. (Hille, 2001). The pore diameter is not uniform however and varies from 8.6 Å at its widest point to approximately 3Å at its narrowest (see Figure 1). Based on sequence analysis, the M2 segments of the pentameric subunits were hypothesized to be the actual channel forming components. This has been supported by labeling with non-competitive inhibitors such as phenylmethylphophonium (Hucho *et al.*, 1986). These studies have specifically identified serine 262 in the nAChR sequence, which is present in the δ subunit of the M2 segment, as being in the pore. This residue is part of the high affinity binding site that is indicative of a pore-lining segment (Galzi *et al.*, 1992).

Also adding to the evidence for the M2 segment lining the ionic pore is the fact that

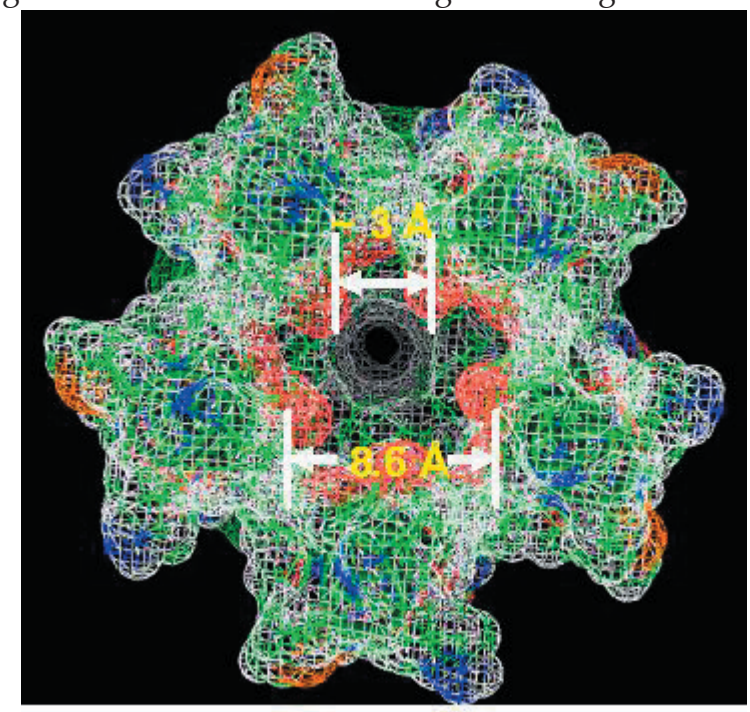

Figure 1: Top View of M2 Pentamer. The pore formed by the homopentamer of M2α subunits. It varies in width from 8.6 Å to approximately 3Å.

the sequence of this segment is highly conserved among homologues and even among different species. The actual pore forming sequence is small, only 23 to 25 amino acid residues in length, and is modeled as an α-helical secondary structure based on electron microscopy studies of intact nAChR. This structure has recently been confirmed for lone M2 segments self-assembled in lipid bilayers by two-dimensional solid-state NMR (Opella *et al.*, 1999). The M2 segments are also amphipathic in nature and they come together at a shallow angle to form the funnel-like pore (Hucho and Weise, 2001). The hydrophobic portions of the helices face the lipid bilayer and act to anchor the peptides in the bilayer while the hydrophilic portion lines the pore region. When gated open, there is a conformational change in the orientation of the M2 segments, allowing permeation of ions through the pore. The channel is selective for cations although it does not discriminate between monvalent cations such as K^+ or Na^+ and even allows permeation of Ca^{2+} to some extent (Hille, 2001). Studies have demonstrated that the vestibules of the nAChR channel are negatively charged, supporting the observation of cation-selectivity. Studies using nAChR samples from the electrical organ of *Torpedo californica* and bovine calf muscle tissue have shown that the δ-segment is the sole determinator of the conductance properties of the nAChR in the different tissue types (Numa, 1989). Thus, when bovine α, β, and γ subunits with a *T. californica* δ-subunit were incorporated into the bovine muscle tissue, there was a significant decrease in conductance than when bovine δ and *T. californica* α, β, and γ subunits were used. While the main portion of the M2 α-helices that form the pore itself are uncharged, the segments have charged residues at either end which form charge rings of a sort when the peptides are assembled into a pentamer. There are three charge rings present in the full receptor, one on the extracellular side of the M2 sequence, one on the intracellular side, and one intermediate within the actual sequence itself (Revah *et al.,* 1991). It has been shown by systemic mutation experiments that channel conductance is diminished as the net charge of one of these rings becomes less negative (Imoto *et* al., 1988).

It has been demonstrated that isolated M2 segments of the nAChR can assemble into alpha-helical bundles (see Figure 2) and function as voltage- gated, cation-

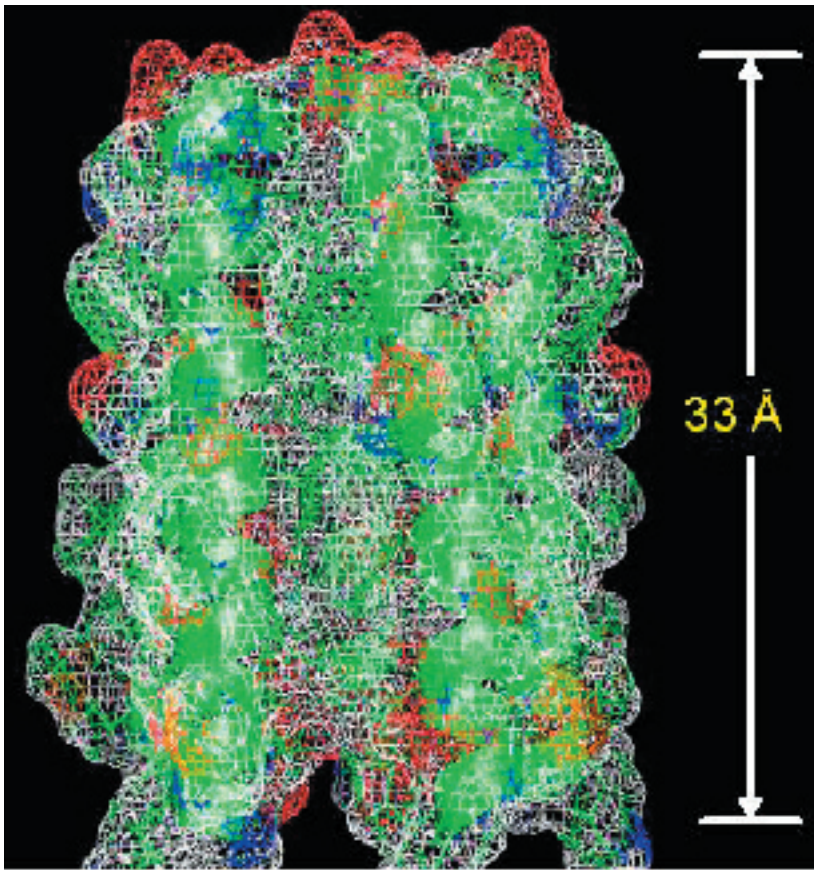

Figure 2: Side View of M2 Pentamer. Homopentamer of M2α subunits. Each subunit forms an α-helix and the length of the ion channel is 33Å. The C-terminal end in this figure is at the top (Sequence from top to bottom of each segment: EKMSTAISVLLAQAVFLLLTSQR.

selective channels in mixtures of 1-palmitoyl-2-oleoyl-*sn*-glycero-3-phosphoethanolamine (POPE) and 1-palmitoyl-2-oleoyl-*sn*-glycero-3-phosphocholine (POPC) (Oblatt-Montal *et* al., 1993). The structure of the individual 23-amino acid M2 helices has been characterized using solution NMR in dodecylphosphocholine (DPC) micelles and a solid-state NMR in bilayers of 1,2-dimyristoyl-*sn*-glycero-phosphocholine (DMPC) (Opella *et al.*, 1999). The alpha-helices described by these studies showed no kinks and channels in the DMPC bilayer were tilted at a relatively shallow angle of 12^{o} relative to the membrane normal. This is useful for getting a general picture of the interaction of the peptide with the lipid environment, however

there were several assumptions made in determining these structures. The solution NMR structure differs from that of the solid-state structure in that it shows a kink in the helix at leucine-11 (Breed *et al.*, 1996). This residue is thought to be important in the gating of the channel.

The amphipathic nature of the individual peptides is thought to be the driving force behind the self-assembly of M2 helices into voltage-gating channels. Looking at the sequence of the M2 δ-subunit we again see the properties of the individual amino acid residues play an important role in the function of the channel. The polar residues, particularly the OH-containing serine and threonine residues, line the pore and play a role in ion affinity and stabilization. The nonpolar, hydrophobic amino acid residues in the sequence act to keep the protein in place in the lipid environment, which leads us to contemplate the effect of lipid selection on channel properties.

Lipids

Lipids are biological molecules that are insoluble in aqueous solutions and soluble in organic solvents. Lipids serve not only as structural components of biological membranes but they also provide energy reserves in the form of triacylglycerols and serve as vitamins and hormones *in vivo*. The membranes made up by lipids are assymetrical, fluid structures capable of fusion and are selectively permeable (Bringezu *et al.*, 2002). They enable specialization of cellular or intracellular functions which by variation in lipid and protein composition, including the transmembrane proteins that form ion channels. The lipid components of membranes are fatty acids, phospholipids, sphingolipids, and cholesterol. Phospholipids form the major lipid part of biological membranes and are composed of two fatty acids plus a phosphate attached to a glycerol. Phospholipids are like triglycerides except that the first hydroxyl of the glycerine molecule has a polar phosphate-containing group in place of the fatty acid. This means that phospholipids have a hydrophilic head and hydrophobic tail. This fact forms the basis for the formation of self-assembled phospholipid bilayers or micelles

in aqueous environments. The head group has a region that is specific for differenct phospholipids. This head group will differ between cell membranes or different concentrations of specific head groups. The fatty acid tails can also differ in length and saturation, but most usually have one saturated and one unsaturated leg of the tail. Sphingolipids are a type of phospholipid derived from sphingosine instead of glycerol. Cholesterol is a major component of cell membranes, particularly those of eukaryotes, and intercalcates between the fatty acid chains, thus lending them rigidity and increased lateral fluidity (Bringezu *et al.*, 2002). Cholesterol also makes the membrane less permeable to small, water soluble molecules and it has been shown to thicken phospholipids bilayers upon insertion.

With regards to the nAChR, it has been shown that the optimal channel function requires the presence of negatively-charged lipids and cholesterol (Sunshine and McNamee, 1992). For this project, diphytanoyl-based lipids were chosen as they work well for planar systems, such as the ones we are using, as well as the fact that they may allow for more highly resistive bilayer formation than natural lipids due at least in part to the presence methyl groups on the fatty acid chains of the synthetic lipids. They are also well-suited for the tethering process that will eventually be used to increase stability in the electronic devices. The synthetic lipid used in all experiments was the diphytanoyl derivative 1,2–diphytanoyl–*sn*-glycero-3-phosphocholine (DPhPC) provided by Avanti Polar Lipids, whose structure is compared to a native lipid in Figure 3. As can be seen, DPhPC is significantly different from the native lipids associated wth nAChR. Thus we undertook a thorough study of the channel forming characteristics of M2 in DPhPC in order to establish the feasibility of changing the lipid environment for optimal sensor design without compromising the functionality of the ion channel.

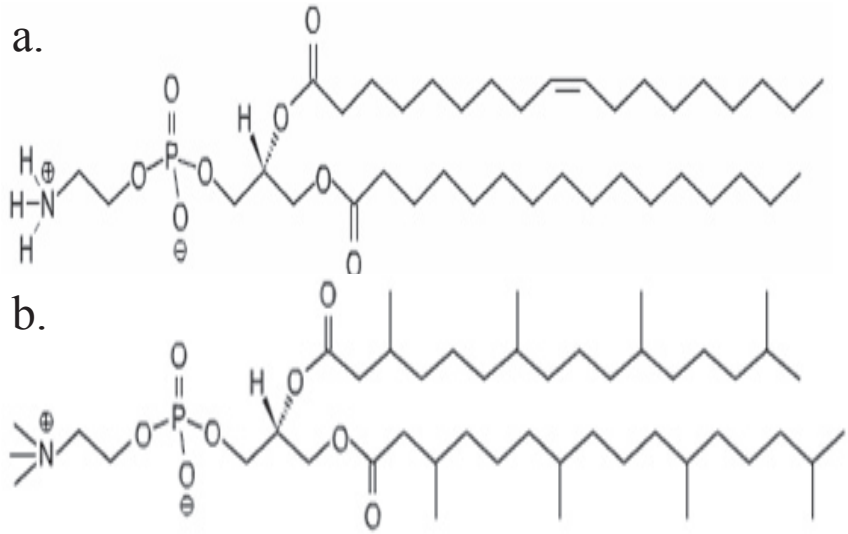

Figure 3: Comparison of Synthetic and Native Lipid Structure. Notice that the fatty acid chains in POPE (a) are unmethylated whereas the synthetic DPhPC (b) is methylated contributing to the additional rigidity of the bilayers they form.

Electrical Properties of Membranes

When attempting to measure the ease of current flow across a membrane, whether due to pores in the membrane or functional ion channels, it is important to understand the physical principle governing the phenomenon. The ease of current flow is referred to as conductance and is usually measured between two conducting electrodes in a salt solution. The conductance is governed by Ohm's Law, which states

$$I = gE$$

where I is the current, g is the conductance, and E is the potential difference across the conducting material, in our case the ion channel. The conductance can be affected in many ways by either changing the properties of the environment or the conducting material. Conductance is increased by increasing the salt concentration using more mobile salt ions, or decreasing the distance between electrodes. Conductance can be decreased by introducing a nonconducting material between the electrodes, moving the electrodes apart, or by increasing the viscosity of the ion salt solution. In the case of the membrane ion channel system, the lipid bilayer acts as a barrier to ion flow and thus decreases the conductivity or reciprocally increases resistivity of the system. Another

important consideration is the fact that a lipid bilayer membrane has a capacitive effect. It plays the role of a dielectic insulator between two conductors, which in this case are the separate salt solution reservoirs on either side of the membrane. It is necessary to consider this capacitance because it plays a central role in the determination of the number of ions that must be transmitted for a current signal to be observed at the membrane (Hille, 2001). The capacitance is defined as the amount of charge that must move from one reservoir to the other to set up a given potential:

$$C = Q/E$$

(where Q is the charge transferred, E is the potential difference, and C is the capacitance). The rate of change of potential due to current flow, I_m, at the membrane is given by:

$$dE/dT = I_m/C$$

The capacitance is relatively constant for a given membrane environment. In terms of membrane properties, the capacitance of the lipid bilayer is given by the equation:

$$C = K\varepsilon_0 A/d,$$

where K is the dielectric constant of the given lipid, ε_0 is the permeability of free space, A is the surface area of one of the lipid layers and d is the distance from one side of the bilayer to the other. The capacitance of cell membranes is estimated to be approximately 1.0 $\mu F/cm^2$ and the capacitance for a simple native lipid bilayer is slightly less at 0.8 $\mu F/cm^2$ (Almers 1978). From these measurements, we can estimate the thickness of a lipid bilayer to be approximately 23 Å, assuming a dielectric constant for hydrocarbons of 2.1 (Hille, 2001). The general effect of membrane capacitance is to slow down the response to any current by a time, τ, that depends on the resistance and capacitance of the membrane. Thus we can express the discharge rate of the membrane "capacitor" as:

$$dE/dt = I_m/C = -E/RC = -E/\tau$$

Solving this differential equation gives us an expression for the potential across the membrane as a function of time, t. Given an initial potential, E_0, this relationship is

$$E = E_0 \exp(-t/RC) = E_0 \exp(-t/\tau)$$

The time constants for the different biological membranes and lipid bilayers can vary significantly, thus the resting membrane resistances can vary in order of magnitude from 10 to 10^6 Ω (Coronado and Latorre, 1983). Thus the number of ion channels open at rest varies significantly from membrane to membrane depending on the properties of the lipids and channels involved. Now we have all of the components to look at the

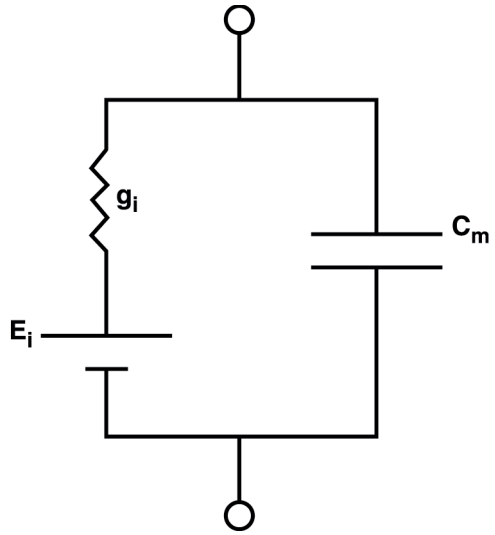

Figure 4: Circuit Model of a Membrane. The electrical properties of a membrane can be modeled using the conductance, g_i, of ions crossing the membrane with a membrane potential, E_i in series. These elements are then in parallel with the capacitance C_m, set up

bilayer/channel environment as a circuit-like model. If we take the ion channel to be a conductor, with conductance, g_i, for a particular ion, i, and the membrane capacitance and electromotive force of the pore to be C_m and E_i, respectively, then the system can be shown to behave like the following equivalent circuit in Figure 4. The driving force of the specific ions, I, is not simply related to E, the potential across the membrane, but

instead is determined by the difference of the total potential and the potential at the pore. Thus the current flow of I through the channel/membrane system is expressed as:

$$I_i = g_i (E - E_i)$$

While this is adequate to a first approximation, many channels have been observed to have non-linear current-voltage relationships when open. This non-ohmic behavior can be due to ionic gradients across the membrane or when the structure of the ion channel itself lacks symmetry. By looking at current versus voltage (I – E) curves, a significant amount of information about the ion channels being observed can be gleaned. For instance, if the curves are linear and pass through the origin, then it can be inferred that either the channels are nonselective if there are multiple salt ions in solution or that there is no gradient set up across the membrane. If the slopes of the I – E curves of a given system increase, it corresponds to an increase in the equivalent conductance and thus an increase in the number of channels in the open state (Hille, 2001). Conductances that show a dependence on voltage are said to undergo rectification. An environment that shows strong rectification usually has channels that are open for some groups of potentials while remaining closed at others.

CHAPTER 2
MATERIALS AND METHODS

Channel Synthesis

The synthetic oligomeric M2 peptide corresponding to the 255-277 segment (EKMSTAISVLLAQAVFLLTSQR) of the δ form of the *Torpedo californica* AChR was prepared via solid-phase methods. The δ form was selected due to the fact that it is well-characterized (Oblatt-Montal *et al*., 1993, Opella *et al*., 1999). Solid-phase chemistry allows for a much less time-consuming synthesis as isolation and purification is not required at every step as in solution-phase chemistry. The synthesis was carried out with PEG-polystyrene resins under continuous flow conditions using FMOC chemistry by the University of Florida protein core facility. The C-terminal end of the peptide with the protected first amino acid residue in the sequence is pre-loaded onto the resin. The next amino acid in the sequence, which was also protected, was activated with an acid fluoride and added to the FMOC-deactivated segment loaded on the resin. A peptide bond was thusly formed between the two amino acids in the chain. Then the excess, unreacted amino acids were washed from the resin and the activation and deprotection steps were repeated with each subsequent amino acid in the sequence until the full peptide was formed on the resin. A schematic of this process is shown in Figure 5.

Next it was necessary to cleave the M2 δ-subunit peptide sequence from the resin. The first step in this process was to wash the resin with approximately 25mL DCM for each gram of crude sample resin through a small sintered glass funnel. The resin was then carefully transferred to a round bottom flask where 10mL of cleavage reagent (90% trifluoroacetic acid (TFA)/ 5% triisopropylsilane/ 5% water) for each

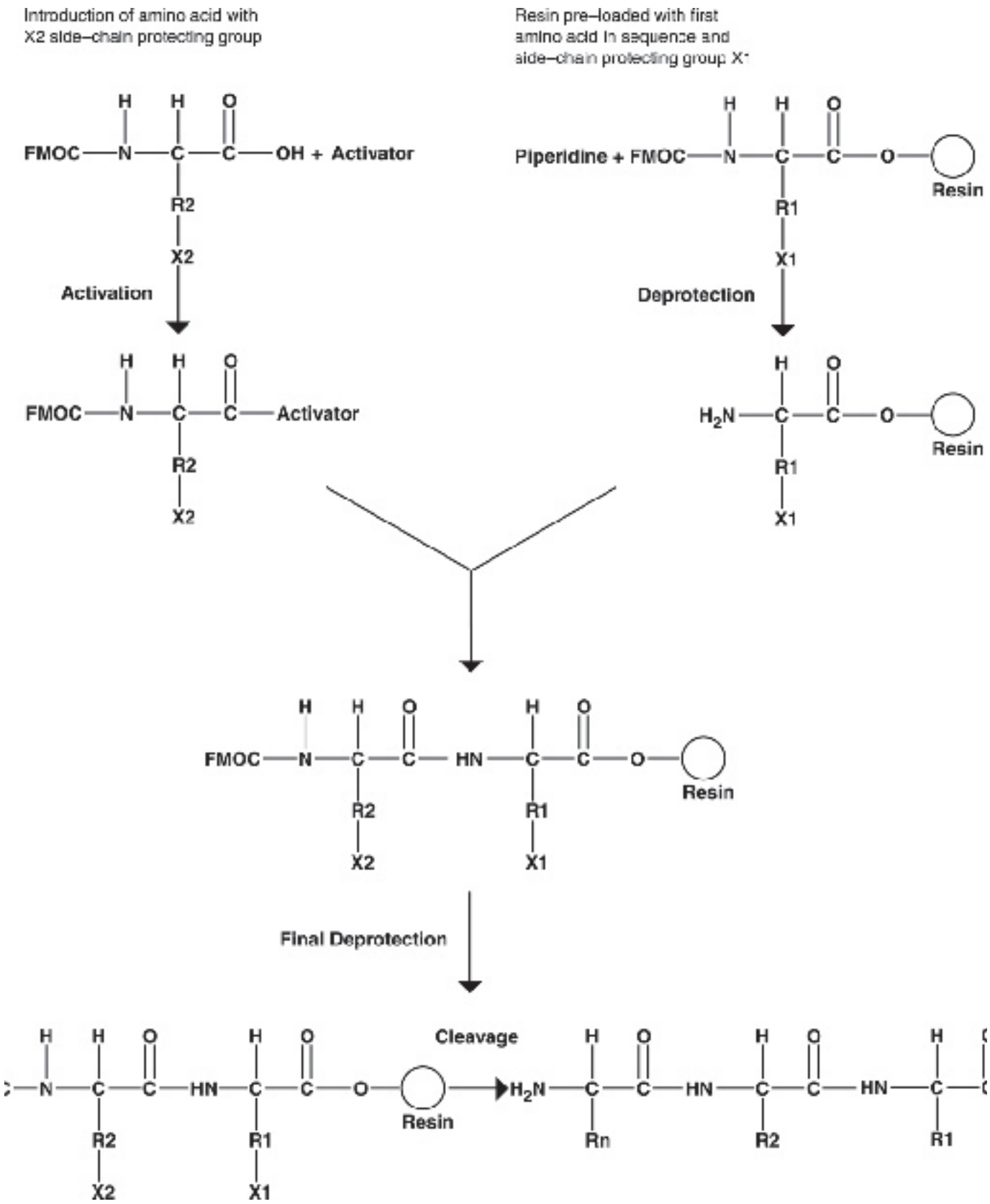

Figure 5: Schematic of Peptide Synthesis.

gram of crude resin sample was added. All spatulas and other transfer tools were washed into the round bottom flask with the same solution to ensure as high of a yield as possible. The flask was then stoppered and stirred. A small stir bar was placed inside the flask to ensure mixing while the reaction occurs. The solution was allowed to react for approximately three hours.

The mixture was then filtered through a sintered funnel and was then washed with 1mL TFA. The total filtrate was concentrated under vacuum at 68°C to approximately 2mL. The concentrated solution was slowly transferred into two Falcon tubes containing 25mL ethyl ether at -20°C. The solutions were then centrifuged, yielding pellets. The ethyl ether was then decanted and the process was repeated three times. Following the washes, the ethyl ether was removed under light vacuum and then placed under high vacuum in a desicator for at least two hours.

Channel Purification and Production

The cleaved peptide was purified using an Äkta Purifier (Amersham Pharmica Biotech) reversed-phase high pressure liquid chromatography (RP- HPLC) apparatus equipped with a silica C_{18} column from Vydac (see Figure 6). This method allows for the separation of peptides with sequences that differ by as little as one methylene group on a single amino acid (Carr, 2002). Unlike small molecules, peptides are too large to partition in the hydrophobic phase stationary phase. Instead, they must be absorbed to the hydrophobic surface of a column. An absorbed peptide remains on the column until the concentration of added organic modifier (usually acetonitrile) reaches the critical value needed for desorption. This critical value is know as the Z number and was first described by Geng and Regnier. The Z number has an extremely narrow region of concentrations that define it and it is very sensitive to the conformation of the protein being desorbed. Once desorbed, the peptide interacts very little with the hydrophobic surface as it elutes off the column. In RP-HPLC, the peptides are separated based on slight differences in the "hydrophobic foot" portions of their sequences and structures,

which is the only region of the peptide in contact with the hydrophobic surface of the column. The foot is strongly correlated with the Z number as it is the only region of the peptide that is involved in the interaction with the organic modifier. In fact, the precise location of the hydrophobic residues in a helical peptide are important in determining the retention time of that peptide in the organic modifier. The absorption/desorption step occurs only once for a given peptide on the column (Carr, 2002). Since peptides are very sensitive to the concentration of organic modifier present, elution gradients are usually set up to maintain precise separation. The polypeptides are sensitive to the concentration of organic modifier used. Relatively small concentration changes in the acetonitrile cause large changes in the retention time. The organic modifier concentration must be maintained precisely and isocratic elution is difficult due to the sensitivity of the polypeptide to changes in the concentration of the modifier solution. Therefore, for RP-HPLC separations, gradient elution is preferable, even with small changes in organic modifier concentration per unit time. Thus a hybrid separation method is indicated: small peptides desorb more quickly with small changes in modifier concentration than small molecules, but more slowly than proteins. In a helical peptide, the exact location of hydrophobic residues greatly influences predicting peptide retention (Yang *et al.*, 1992).

The hydrophobic surface upon which the polypeptides adsorb is the HPLC column, which is a stainless steel tube filled with spherical particles of small diameter. The particles used are generally silica with highly uniform sites and surface areas, which have been modified for use as adsorption agents by silane reagents to make them hydrophobic. The smaller the diameter of the adsorbent particles, the higher the specificity and resolution of the peptide fractions eluted from the column. The adsorbents used are porous in nature and the polypeptides enter a pore to be adsorbed and separated. RP- HPLC has been effectively used for polypeptide separations since large-pore silica particles of about 300 Å were engineered. Now this is the size most

commonly used, but some smaller peptides can also be separated using particles of 100 Å (Carr, 2002).

Usually, a linear aliphatic hydrocarbon of 18 (C_{18}), eight (C_8) or four (C_4) carbons is used as the hydrophobic group. Peptides and small proteins of size less than 5,000 daltons are usually separated using C_{18} columns. In order to produce RP-HPLC adsorbents, hydrocarbon chlorosilanes with one reactive chlorine are added to the silica matrix (Carr, 2002). As these have a single point of attachment with the matrix, they are called monomerically bonded phases. If chlorosilanes with multiple reactive chlorines are used, the product is known as a polymerically bonded phase, in which the individual chlorosilanes are crosslinked and form a silicone polymer on top of the silica matrix, with multiple hydrophobic chains attached. Monomerically and polymerically bonded phases exhibit some differences in sensitivity for separating polypeptides, even though they have similar hydrophobicities and separation. Mild conditions of acidic pH and room temperature are ideal for running silica-based HPLC but extreme conditions such as high pH or high temperatures will rapidly degrade silica columns. Polystyrene-divinylbenzene, a synthetic polymer, provides a very sturdy alternative matrix for separations. Synthetic polymers provide the advantage of not degrading at extreme changes in pH. Therefore very acidic or basic solutions can be used to clean the apparatus. Using very strong reagents to wash the column does not adversely affect the column performance, as indicated by an examination in which peptides chromatographed before and after washing with both strong acid and base had similar peak shape, retention, and resolution.

Column length does not significantly affect the separation and resolution of proteins, because both adsorption and desorption largely take place near the top of the column (Yang *et al.*, 1992). Short columns (of 5-15 cm) are frequently used for protein separations. Small peptides are better separated on longer columns, and columns of 15-25 cm are used for the separation of synthetic and natural peptides. Column length is

proportional to column back-pressure. While the column diameter does not affect peak resolution, it does affect sample loading. The detection sensitivity is increased when the column diameter is reduced, because the flow rate is reduced, and therefore less solvent is used (Rivier *et a.l*, 1984).

Aqueous solvents contain an organic modifier and an ion-pair reagent or buffer. The organic solvent is used to desorb polypeptide molecules from the adsorbent hydrophobic surface. This is achieved by slowly increasing the concentration of solvent until the polypeptides desorb and elute. This results in the sharpest peaks and best resolution. The most commonly used organic modifier is acetonitrile (ACN) for several reasons: it is very volatile and therefore easily removed from fractions; its low viscosity minimizes back-pressure; it has little UV adsorption at low wavelengths; it has proven to be consistently reliable in RP-HPLC separations (Carr 2002, Yang *et al.*, 1992).

Low-gradient slopes are preferable to isocratic elution, as a uniform concentration of organic modifier produces unacceptably broad peaks (Yang *et al.*, 1992). The slope of a typical solvent gradient is 0.5 to 1% per minute increase in organic modifier solution. To maximize resolution, very shallow gradients (from 0.5 to 0.1% per minute) can be used. Extremes in organic modifier concentration are to be avoided in order to have the best equilibration and reproducibility. Gradients should be begun at no less then 3 to 5% organic modifer concentration, and should not exceed 95% organic modifier. The higher concentration of organic modifier may remove all the water in solution, thus making column equilibration more difficult (Carr, 2002).

The slope of the solvent gradient may affect peptide selectivity and resolution between peptide pairs because of the slight differences in the way that some of the peptides interact with the reversed-phase surface. The purpose of the ion-pairing reagent/buffer is to set the eluent pH and interacts with the polypeptide to enhance the separation (Hoeger *et al.*, 1987). Trifluoroacetic acid is the most commonly used ion-pairing reagent because it is volatile and can be easily removed from fractions, it has

very little UV adsorption at low wavelengths, and it has proven reliable in RP-HPLC separations. Using concentrations of TFA at lower than 0.1% when chromatographing proteins may degrade peak shape. As the solvent environment changes from aqueous to non-aqueous the dielectric constant changes, affecting π-π electron interactions, which affect the 190-250 nm region of the adsorption spectrum, and causes a baseline shift (Rivier *et al.*, 1984). Adjusting the wavelength as close to 215 nm and putting 15% less TFA in the organic modifier solvent than in the buffer solvent reduces or eliminates the baseline drift due to TFA spectral adsorption. Using high-quality TFA is also essential, as low quality or aged TFA may cause the presence of spurious peaks.

Polypeptide separations are not very affected by flow rate. The eluent flow rate may affect the resolution of small peptides because their behavior in RP-HPLC columns is between that of proteins and small molecules (Yang *et al.*, 1992, Carr, 2002). Adsorption and sensitivity increase with lower flow rates because smaller volumes of solvent are used. This is also why narrowbore HPLC columns increase detection sensitivity: they are run at low flow rates. However, while it increases the amount of solvent to be removed from the purified sample, high-flow rates may improve the solubility of hydrophobic polypeptides (Rivier *et al.*, 1984).

RP-HPLC is used to purify microgram to milligram quantities of polypeptide samples for research purposes. For large-scale preparation, however, some other constraints exist as well (Rivier *et al.*, 1984). The same ion-pairing agents commonly used for analytical purposes are not always as practical for large-scale chromatography. When loading a large-scale preparation, some factors that need to be considered are: low sample loads yield best resolution, only small quantities are purified per run; the purity of the sample is expressed in terms of percentage of total weight of final purified product; and the yield is the percentage of final purified product per total amount of polypeptide present in original sample (Yang *et al.*, 1992). Higher resolution enables maximum yield. Thus several factors must be balanced. The three measures of sample

capacity in a RP-HPLC column are: loading capacity with maximum resolution, practical sample loading capacity, and maximum amount of polypeptide that the column will bind (Carr, 2002).

Figure 6: RP-HPLC Apparatus.

The solvents used for the RP-HPLC purification were water with 0.3% TFA and HPLC-grade acetonitrile (ACN) with 0.3% TFA. M2 isa a highly hydrophobic peptide and is only minimally soluble in water. Consequently, the crude sample was prepared for injection onto the column by first dissolving 5-15 mg of peptide in 0.2 mL TFA. Once dissolved, 0.2 mL trifluoroethanol (TFE) was added and the solution was mixed well. Then 0.6 mL ACN was added to the solution, which turned cloudy at this point in the preparation. Next, 4 mL 30:70 ACN: H_20 was added to the solution. The solution was spun down so that any excess undissolved peptide could be recovered. Then the aqueous supernatant was removed with a microsyringe and was then injected onto a 5 mL sample loop for RP-HPLC preparation. A gradient of 40% to 60% of the organic modifier (ACN and 0.3% TFA) was used for separation. Wavelengths of 220 nm to 280 nm were used to observe the absorbance of fractions of the desorbed protein segments as they came off the column. Two major peaks were observed: one at between 47-49%

organic modifier, and the other between 53-55% organic modifier. 8 mL fractions from 45% to 60% organic modifier were collected in Falcon tubes. Then each individual fraction was placed in a round-bottom flask, and the ACN and any trace of TFA were removed using the Roto-Vap under vacuum with a water bath at a temperature of approximately 50°C and Roto-Vap coolant water at 4°C. Once the samples were concentrated to approximately half their original volume, they were removed by glass pipette and put back into the original Falcon tubes. For each fraction, the round-bottom flask was rinsed with deionized water and the water was pipetted into the corresponding Falcon tube to ensure maximum yield. If the same round-bottom flask was used for multiple concentrations, it was rinsed three times alternating with methanol and deionized water. The samples were then frozen at -30°C. Once frozen, the caps of the Falcon tubes were removed, and the tubes were sealed with parafilm. Then three small puncture holes were made in each parafilm seal and the tubes and caps were placed in the glass lyophilization container. The samples were lyophilized under vacuum at less than 100mTorr until only a white powder remained.

In order to identify which of the major peaks contained the correct M2 sequence, the samples were prepared for mass spectrometry. First, a solution of ACN with 0.1% TFA and deionized water with 0.1% TFA in a one to one volumetric ratio was prepared. A small sample of the lyophilized powder for each major peak was dissolved in 90 µL of this solution to yield an approximate concentration of 0.1 µM peptide. Then the solution was diluted tenfold with the 1:1 ratio of ACN: H_2O (both with 0.1% TFA). And then the diluted fraction was again diluted with the same solvent. Next a cyano-4-hydroxycinnamic acid (CHCA) matrix was prepared by dissolving 10 mg sample in 1X methanol in 0.5 mL of solvent. The solution was then vortexed, and methanol was then added until the solution was saturated. Then the matrix solution was centrifuged and the supernatant was carefully removed. The matrix and the diluted sample were mixed in a 10:1 ratio. Then 1 of 2 µL of solution for each sample was placed on a specific

location on a MALDI plate. The CHCA matrix was placed on a few of the MALDI locations alone for use as a blank. First the blanks were tested to see if good resolution could be obtained. Then the other samples were tested on the MALDI plate, with the higher concentration samples giving the best resolution. The results show the expected molecular mass of 2522.29 amu for the sample collected at approximately 48% organic modifier during the PR-HPLC. The other major peaks had molecular masses of 2409.38 amu and 2395.31 amu which represented peptides missing an amino acid residue in the sequence, most likely valine and lysine, respectively.

To verify the sequence and concentration of the peptide, lyophilized samples of the different peak fractions were dissolved in approximately 100 µL TFE for each 1 mg of sample used. Each sample was then heated in a water bath at about 40-50^{o}C for approximately 2 hours. Then the solutions were diluted to 2 mL with H_2O. Then 100µL of this dilute solution was further diluted to 1 mL with H_2O. 100 µL of this solution was sent to the protein core facility at the University of Florida to have amino acid analysis performed. Also, this solution was used to obtain UV spectra from 200-400 nm. QuartzUV cells were used because residual peaks near 200 nm were appearing for blanked solutions when methyl crylate cells were used. The results of the amino acid analysis were in close agreement for the expected composition of the M2 peptide. The predicted peptide sequence had an average percent error of 12.73% compared to the known composition which is within the error of typical amino acid analysis. The predicted concentration of the sample was 69.8 pmol/ µL L or 0.16 µg/µL.

In order to be able to determine concentrations of M2 solutions with greater ease via UV absorbance, it was necessary to calculate extinction coefficients to be used with the Lambert-Beer law. The law can be stated as

$$A = \varepsilon c l$$

where A is the absorbance, l is the path length, c is the concentration, and ε is the extinction coefficient. Extinction coefficients for absorbances at wavelengths of 208 nm,

214nm, and 220nm were calculated using the UV spectra of a known concentration of M2 in deionized water. This concentration was determined by amino acid analysis and the path length for the glass cells was 1 cm. Using the Lambert-Beer Law, the concentration of all subsequent M2 samples was determined. The coefficient at 208 nm was determined to be 6.517×10^{-3} Au µL/pmol cm or 2.810 Au µL/µg cm. At 214 nm, the coefficient is 3.823×10^{-3} Au µL/pmol cm or 1.638 Au µL/µg cm. And the values for the coefficient at 220 nm were 2.244×10^{-3} Au µL/pmol cm and 0.961 Au µL/µg cm. Once concentration was determined for a particular sample, it was then frozen, lyophilized, and then carefully brought up in an equal volume of 30:70 methanol (MeOH): chloroform ($CHCl_3$) solution. The synthetic DPhPC lipids were also brought up in solution of the same solvent ratio and then solutions of various molar mixing ratios were prepared from these stock solutions.

Circular dichroism experiments were done using M2 in different solvents to determine the secondary structure of M2 in solution. Solutions of the following: 1:1 TFE:H_20, 30:70 TFA: H_20, 30:70 MeOH: H_20, 30:70 TFA: $CHCl_3$, and 30:70 MeOH: $CHCl_3$, each with and without M2 peptide present were prepared. Samples of 400µL were used for each run in a cuvette with cell length 0.1 cm. Samples containing chloroform or TFA scattered the input light such that no useful data could be obtained as a clear spectrum could not be observed. The molar ellipticity as a function of wavelength was plotted for the M2 in solution, for samples where spectra could be obtained. Molar ellipticity can be expressed as number of millidegrees of rotation of polarized light divided by the product of the number of amino acid residues in the peptide, the concentration of the peptide, and ten times the cell length. The results of these experiments, after buffer subtraction, showed that M2 was in an unstructured, random coil conformation in the 30:70 MeOH: H_20 solution. This is what would be expected for a non-aggregating amphipathic peptide.

Monolayer Formation and Isotherm Data Acquisition

Named after Irwin Langmuir, who in the late 1910's was the first to perform systematic studies on floating monolayers in water, Langmuir films are rapidly growing in importance in the scientific community. The name Blodgett was added several years later when Katherine Blodgett gave a detailed description of monolayer transfer. Lagmuir films usually refer to floating monolayers, and Langmuir-Blodgett films refers to a monolayer attached to a solid substrate.

The sustaining force that causes the formation of monolayers in such a system is surface tension (Roberts, 1990). Molecules in a liquid experience attractive forces in all directions. The molecules on the surface of the liquid experience stronger intermolecular forces with other molecules of the liquid as opposed to the air molecules at the interface. Therefore the liquid will automatically minimize the surface area exposed to the air. Having a minimum surface area exposed to the air also lowers the energy of the liquid molecules, which is favorable. The more polar the molecules of the liquid, the stronger the intermolecular forces involved, and the higher the surface tension will be. Any contamination will affect the surface tension, and therefore researchers should avoid any contamination (Shaw, 1980). Also, increasing the temperature will lower the surface tension.

Surfactants are surface active agents and they consist of a hydrophilic portion and a hydrophobic, non-polar portion. As they are contain segments soluble in both polar and non-polar solvents, amphiphilic or amphiapathic molecules tend to accumulate at interfaces (Laughlin, 1994). Altering the size of both the hydrophilic and hydrophobic portions will produce a wide variety of self-assembled structures, but all of them come about due to a reduction in free energy. Langmuir films are a one-molecule-thick insoluble monolayer that come about when an amphipathic substance is spread on the surface of water (Roberts, 1990, Binks, 1991). The polar ends stay on the water side of the interface, and the non-polar ends point up. Usually, the hydrocarbon

chain, the non-polar portion, must be at least 12 hydrocarbons in order to form a monolayer rather than a micelle (Harkins, 1952). However, if the hydrocarbon chain is too long, the molecules will crystallize on the surface rather than forming a monolayer. Therefore, a delicate balance must be attained.

Water has a very high surface tension compared to other liquids, and therefore makes a good subphase for monolayer experiments. The procedure for forming a Langmuir film is as follows: first place amphipathic solution (in a non-polar solvent) with microsyringe on the surface of the subphase solution; as solvent dissolves, a monolayer forms. This monolayer is considered a "gas" because the molecules are quite far apart (Roberts, 1990). Barriers on the far ends of the water trough are brought closer together very slowly. As the surface area of the monolayer decreases, the surface pressure increases and the molecules repel one another. The equation

$$\Pi = \gamma - \gamma_0$$

for surface pressure, Π, is a two-dimensional reckoning of pressure, where γ is the surface tension in absence of a monolayer and γ_0 is surface tension when the monolayer is present.

The trough for making a Langmuir monolayer is made of Teflon so as to prevent any leakage of the subphase (Adamson, 1976). Water is circulated in channels underneath the Teflon trough in order to maintain the proper temperature. The surface area of the trough can be adjusted with movable barriers. Each barrier is heavy enough to prevent to prevent any leakage of the monolayer underneath the barriers. The Wilhehmy-plate method is used to measure the surface pressure. A schematic of this system is given in Figure 7. In this method, a plate is suspended partially immersed in the subphase. The force exerted by the surface is converted into surface pressure by accounting for the size of the plate (Gaines, 1966, Robert, 1990). The forces on the plate are surface tension acting downward, gravity, and buoyancy acting upward.

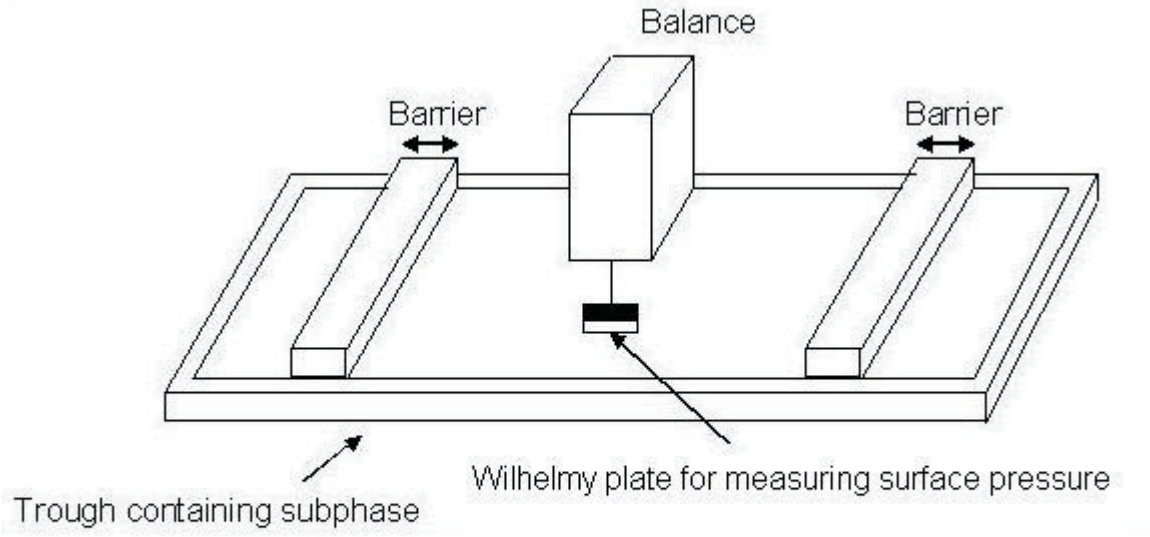

Figure 7: Schematic of Langmuir Trough.

To measure the net downward force, F, on a plate with dimensions l_p, w_p, and t_p, of material with density ρ_p, immersed to a distance of h_l in a liquid of density ρ_l, the following equation is used

$$F = \rho_p g\, l_p\, w_p\, t_p + 2\gamma(t_p w_p)(\cos\theta) - \rho_l g\, h_l\, w_p\, t_p$$

where γ is the surface tension of the liquid, θ is the contact angle of the liquid on the plate, and g is the gravitational constant. Then the surface pressure must be determined by comparing the net force with the monolayer present and without the monolayer. If the plate is completely submerged, and θ is 0, use the equation:

$$\Pi = -\Delta\gamma = -[\Delta F/2(t_p + w_p)] = -\Delta F/2w_p, \text{ if } w_p >> t_p.$$

Thus, the thinner the plate, the more sensitive the result will be (Gaines, 1966). In order to keep the surface pressure constant, it is possible to use a computer controlled feedback system, which is in fact how our system is set up.

A surface-pressure-area isotherm is one of the best indicators for the monolayer properties of an amphipathic material (Chattoraj and Birdi, 1984). It is known as an isotherm because it is performed at constant temperature. Isotherms are recorded

by measuring the surface pressure as the surface area is decreased by compression of the monolayer. Sometimes, many repetitions are required to find isotherms that are reproducible as small variations in the system variable or the presence of contaminants can have a significant effect on the monolayer behavior. Several areas of constant slope become evident upon examination of an isotherm. The regions are known as phases. Generally, the phase behavior is determined by the physical and chemical properties of the amphiphile, the subphase composition, and temperature (Roberts, 1990, Binks, 1991). The length of the hydrocarbon chain and the magnitude of any other forces existing between the headgroups determines the various monolayer states. The surface-pressure-area isotherm can be condensed by increasing the chain length, which in turn increases attraction between molecules. A nomenclature system was developed by W.D. Harkins in which monolayers in the gaseous state are given names (G) (Roberts, 1990). When compressed they will transition to the (L_1) state known as the liquid-expanded state. When compressed further the liquid transitions to the liquid-condensed state (L_2) and when condensed further it becomes the solid state (S). However, if the monolayer is compressed any further it will collapse. The collapse is evidenced by a rapid decrease in surface pressure or a break in the isotherm. Several other critical points exist in the surface-pressure-area isotherm, such as A_i which is apparent by the pronounced increase in the surface pressure as well as surface pressures at which phase transitions occur between the other states, marked by a change in slope.

The mixing behavior of M2 and DPhPC was studied using Langmuir monolayers as described above. Surface-pressure-area isotherm data was gathered using a KSV 5000 Langmuir trough with dimensions 44 cm x 7.35 cm and a Wilhelmy balance (see Figure 8). The 30:70 MeOH: $CHCl_3$ spreading solution previously

described was used because the MeOH solvent allowed for complete solvation and prevention of aggregation of M2 and the $CHCl_3$ allowed for quick evaporation leaving only the peptide/lipid molecules on the surface.

Figure 8: Langmuir-Blodgett Apparatus.

The subphase solution was composed of 500mM KCl, 1mM $CaCl_2$, 5mM HEPES, adjusted with KOH to pH 7.4. The monolayers were formed by compressing the peptide/lipid mixture between the barriers of the trough with a compression speed of 5mm/min at a temperature of 23°C. It is important to note that the platinum Wilhelmy plate was heated before use in order to make the surface rough so that it would act more hydrophilic and allow for a smaller contact angle at the surface. Also, surface pressure area isotherms were obtained for pure M2 samples deposited on the air-water interface. Compression, decompression, and recompression cycles below the collapse pressure were performed by moving the barriers to minimize and maximize the total surface area at the interface on which the molecules can orient themselves in order to determine the elasticity of the monolayer.

Brewster Angle Microscopy

When looking at the angle of incidence of non-polarized light on a flat insulating surface, at one specific angle all of the reflected light waves are polarized into a single

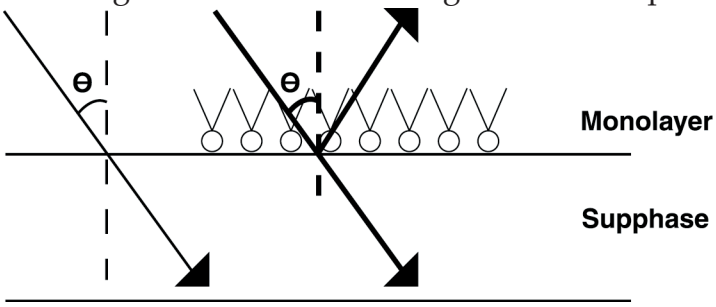

Figure 9: Principle of Brewster Angle Microscopy. When incident light reaches the subphase interface (left) it is transmitted and refracted toward the membrane normal. However, the addition of a monolayer at the air-water interface allows for reflected, polarized light at the specific Brewster Angle.

plane. This angle is known as Brewster's angle. It can be calculated using the following equation:

$$n = \sin(\theta_i)/\sin(\theta_r) = \sin(\theta_i)/\sin(\theta_{90\text{-}i}) = \tan(\theta_i)$$

where n is the refractive index of the medium from which the light is reflected, θ_I is the angle of incidence, and θ_r is the angle of refraction (see Figure 9) . It is therefore very easy to calculate the refractive index of an unknown substance. Snell's law is inapplicable for opaque materials with a high absorption for transmitted light, so

Figure 10: Brewster Angle Microscope.

this technique is especially helpful. Also, this technique determines the amount of polarization, and can be used to establish what phase the monolayer is in. The apparatus used is shown in Figure 10. Brewster Angle Microscopy was used in conjunction with the Langmuir-Blodgett conditions described above in order to get a qualitative picture of the morphologies of the mixtures at the interface.

Patch Clamp Recordings

The patch clamp method for observing single-channel activity was first developed in 1976 by Neher and Sakmann. The patch refers to either a full or partial attachment of membrane or lipid bilayer to the tip of a micropipette that encases a microelectrode that can be used for detecting small electrical signals. There are two types of clamps that can be applied to cell membrane or lipid bilayer. The first is maintaining a forced current through a membrane patch and observing the potential difference across the membrane. However, more commonly used for smaller systems is a voltage clamp, in which a defined potential difference is applied across the membrane and the corresponding current flow is measured. What is essentially created is an equivalent circuit whose components are made up of the lipid membrane, the micropipette, and the subphase solution. This equivalent circuit is shown in Figure 11. In order to observe channel function within the lipid environment, a proper seal must be made that separates the solution in the micropipette, which acts as a conductor, and the subphase (Hille, 2002). This can be done either by bringing the micro-pipette tip against the membrane of a vesicle or a whole cell or by creating a bilayer at the tip through a method known as tip-dipping. As was discussed in the introduction regarding the electrical properties of membranes, the resistance observed at the tip depends on the resistance of the lipid layer itself as well as on the capacitive effect of the membrane. The tip resistance is also affected by leak resistance, which reduces the effective resistance of the patch as well as the capacitive effect of the glass pipette. Single channel measurements were made using the tip-dipping patch clamp method (Coronado and Latorre, 1983, Suarez-Isla,

Wan, *et al*, 1983). First, the micropipettes used to house the electrode were prepared using a Flamming/Brown Micropipette Puller (Model 97, Sutter Instruments Co.) with a heated filament. The micropipettes were pulled to defined micron-scale apertures of approximately 1 μm^2, as verified by bubble-rate test. Tip-dipping experiments were performing in a circular Teflon trough that could be manipulated vertically. Also, some experiments were done using a three-axis manual micro-manipulator. The subphase solution used was composed of 500 mM KCl, 5 mM HEPES, and 1 mM $CaCl_2$, made with milli-Q water and brought to pH 7.4. Bilayers of DPhPC with incorporated

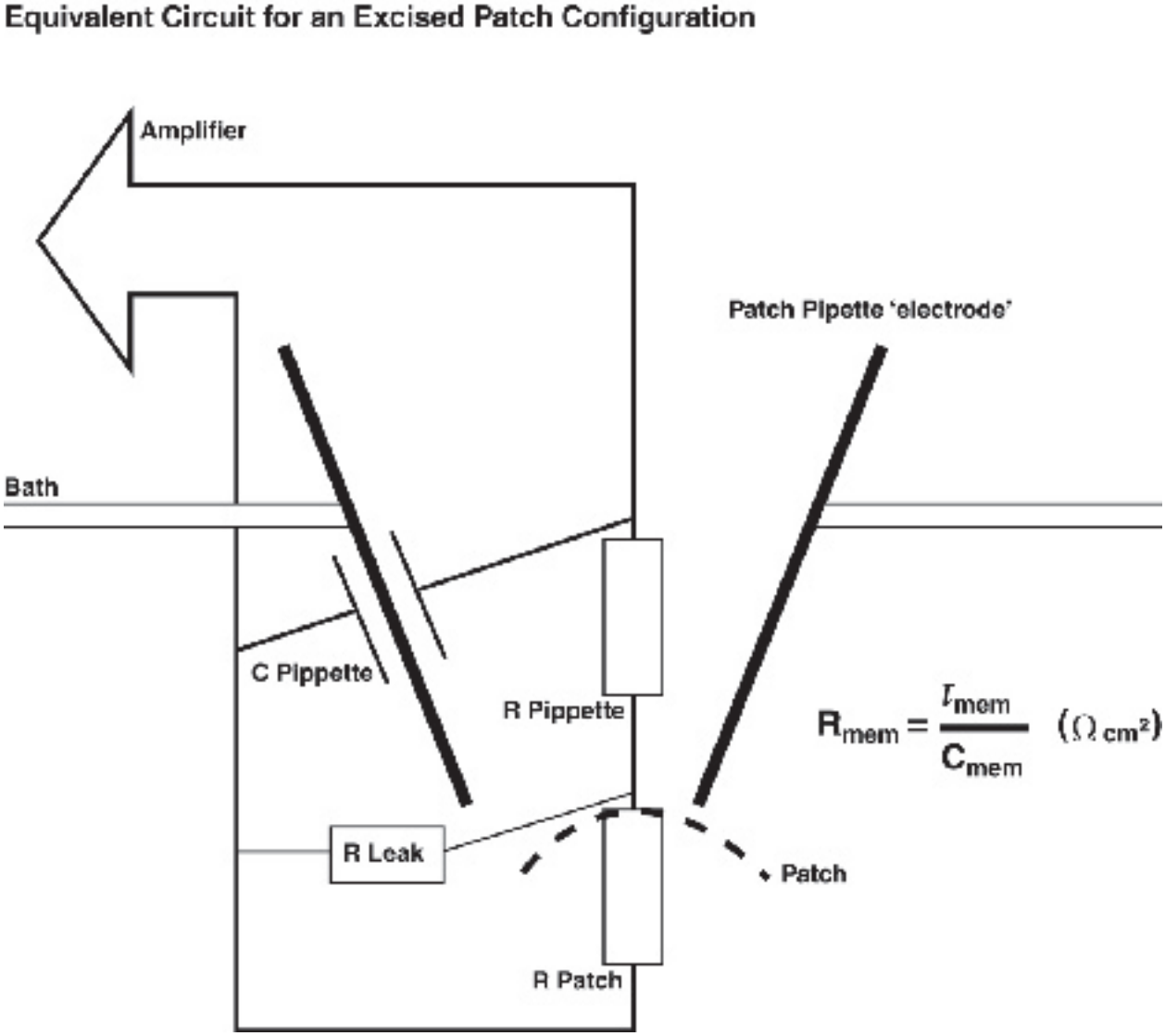

Figure 11: Excised Patch Configuration. The electrical properties of the micropipette and the membrane must be considered when making patch recordings. The membrane resistance, which is important for determining the presence of a seal at the micropipette tip, can be expressed in terms of the membrane capacitance and the time constant, $\tau_{mem,}$ of the bilayer. Adjustments are marked at the amplifier to counteract the effect of pipette resistance and capacitance.

M2 channels were created at the tips of the micropipettes (see Figure 12). In Step A, the DPhPC monolayer with incorporated M2 is raised toward the micropipette, where the solution inside the tip is at positive pressure. In Step B, the tip pierces the monolayer and some of the lipid molecules adhere to the outer surface of the micropipette. Then the positive pressure is released and the trough is slowly moved away from the pipette as seen in Step C. A slight suction is applied to ensure that the proper monolayer seal is

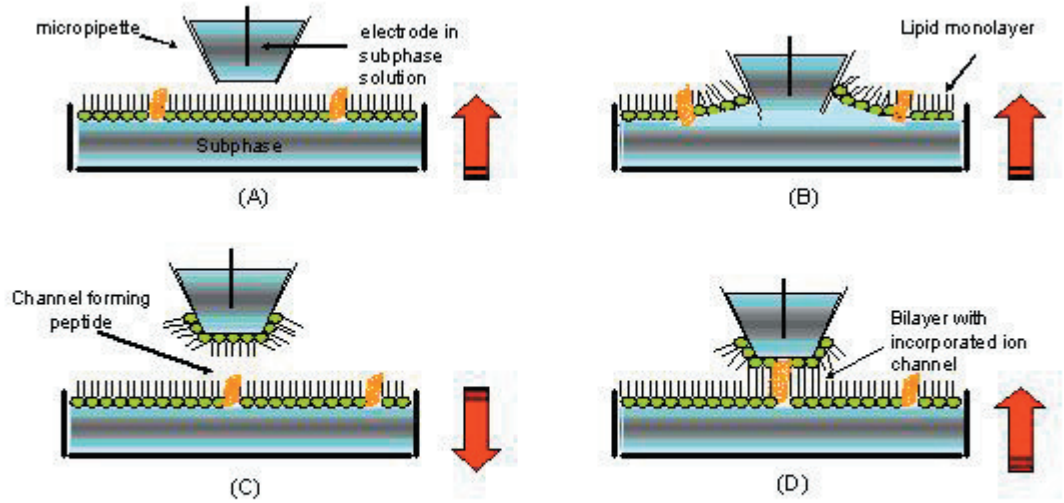

Figure 12: Schematic of a Tip-dipping Procedure. In step A, the DPhPC monolayer with incorporated M2 is raised toward the micropipette, where the solution in the tip is at positive pressure. In step B, the tip pierces the monolayer, and some tf the lipid molecules adhere to the outer surface of the micropipette. Then the positive pressure is released and the trough is slowly moved away from the pipette. A slight suction is applied in order to ensure that the proper monolayer seal is produced at the tip when the micropipette is exposed to the air. Finally, as depicted in step D, the tip is dipped back into the monolayer, on the subphasesurface, creating a bilayer seal on the order of gigaohms.

produced at the tip when the micropipette is exposed to the air. Finally, as depicted in Step D, the tip is dipped back into the monolayer on the subphase surface, creating a bilayer seal with a resistance on the order of giga-ohms. In setting up the patch-clamp apparatus, the first step is to find an area that has low propensity for vibration. Ground-floor laboratory space is ideal, as upper stories have a tendency to amplify vibrations from other parts of the building. During the initial months of this work, we

had to use a non-ideal space on an upper floor. However, eventually, we were able to gain access to ground-floor space. The next step is to set up a sturdy base for the patch-clamp apparatus to rest on. The space should eliminate vibrations as much as possible, and we made multiple efforts to reduce vibrational effects. Cinderblocks were used as the main base, with flat wood planks on top. Then an inner-tube air cushion was placed at each corner of the planks. Next, a large wooden container filled with either cement or sand was placed on top of the cushions. Also used in some cases was a microvibration table which rested on the cement surface of the base. A steel base plate was then placed on top of the microvibration table. The base of the apparatus is shown in Figure 13.

Also of importance is reducing the amount of electrical noise in the vicinity of

Figure 13: Base Structure of Tip-Dipping Apparatus. Notice the grounded steel plate set on the microvibration table. The air cushion can be seen between the cinder block legs and the sand-filled base box.

the amplifier head stage. This is achieved through the use of the Faraday cage, which is constructed of conductive material. The principle is that any outside electrical signal will be prevented from entering the inside of the cage due to the fact that the electrons free to carry the signal can only travel on the outer surface of the conductor. Our

Faraday cage was constructed of copper mesh with steel corner connectors. Once this vibration

and noise-free environment was established, the head stage of the patch-clamp amplifier was secured above the base plate and attached to the micro-manipulator. A Langmuir-Blodgett trough base was placed above the base plate to serve as a movable foundation for the experiments, as shown in Figure 14. All metallic and electrical objects within the cage, including the base plate and the head stage, were grounded by connecting them to the cage itself. The amplifier, signal digitizer, and the manipulation controls were kept outside of the cage, as shown in Figure 15.

The first set of experiments was used to verify that channels were forming functional voltage-gated structures in the lipid environment. An ionic gradient was set up across the bilayer formed at the tip by placing a solution composed of 750 mM KCl, 5 mM HEPES, and 1 mM $CaCl_2$ at pH 7.4 in the pipette. If the peptides come together and function as a voltage-gated channel, it would be expected that in the absence of an applied voltage across the membrane, no current flow would be observed. If, however, there were

Figure 14: Faraday Cage and Full Apparatus. The copper Faraday cage can be seen covering the patch-clamp head stage. There is also a plastic covering surrounding the cage to prevent dust and other debris collecting in the sample trough.

Figure 15: Periphery Patch Clamp Equipment. Above the Faraday cage, the trough controller and data digitizer can be seen.

leaks in the membrane, or the peptides were forming non-gated pores, then current flow would be observed as the potassium ions traveled down the gradient to establish equilibrium. The software used for the data collection and analysis was the Axon Instruments pClamp 9.0 package. In order to understand the gating mechanism and any changes that might occur due to changes in the lipid environment, step-function protocols were established. These protocols involved applying a set voltage for 5-10 seconds and increasing from -200 to 200 mV in 20 mV steps or from 0 to ±100mV with steps of 10 mV. Similar experiments were done in the absence of the gradient. Also of interest was to observe the function of inserted channels over long periods of time. In order to do this, a gap-free protocol was used. In this case, there was no set time for a particular recording. The software was set to record and the voltage clamp at the membrane was altered manually between -200 and 200 mV. Experiments were performed with protein to lipid ratios of 1:100, 1:1000, and 1:10000 for lipid compositions of pure DPhPC, 3:1 POPE:POPC, 3:1 POPE:POPC with 10 mol% cholesterol, 3:1 POPE:POPC with 25 molar percent cholesterol, and3:1 POPE: POPC with 30 molar percent cholesterol. For all experiments, between 4 and 8 µL of M2 lipid solution were spread on the surface of the subphase using a microsyringe.

This corresponds to approximately 2 to 4 times the amount necessary to cover the surface area of the subphase in the Teflon trough exactly, to ensure that at least a single monolayer covered the entire surface. It is estimated at these concentrations that there are on the order of tens to hundreds of single channels present in any given tip.

CHAPTER 3
RESULTS AND DISCUSSION

First let us look at surface-pressure-area isotherms of pure M2δ peptide. As it is amphipathic, we might predict that its behavior would be comparable to that of other amphipathic molecules such as lipids. Looking at the isotherms, we see that they have a shape that supports this proposition. Three distinct kinks occur in the curve, indicating that the peptides on the surface are present in three separate phases before collapsing. The area per molecule at these different phases can be estimated by taking the slopes of the curve at each of the phase transitions and examining where the slopes intersect with the x-axis, which measures area per molecule. From these data we are able to determine area of onset. The onset area is the area per molecule at the beginning of a particular phase. The limitation area is the area per molecule just before the next phase transition. Figure 16 depicts the phase transitions for M2 applied at a concentration of 0.0625 mg/mL in 30:70 MeOH: Chloroform. Under these conditions, the area of onset is 268 $Å^2$ and the film remains in this first phase, which is analogous to a gas phase (G). Once the surface pressure is increased to about 5.9 mN/m, we see transition to the next phase, termed the liquid-expansion phase (L_1). Again, the area of this phase is determined by the slope of the curve, following the corresponding phase transition point. This area was determined to be 194 $Å^2$ and remained in this phase between surface pressures 6.7 and 28 mN/m. The final phase is present above 30 mN/m until collapse at approximately 40 mN/m. It has an area of 136 $Å^2$ corresponding to

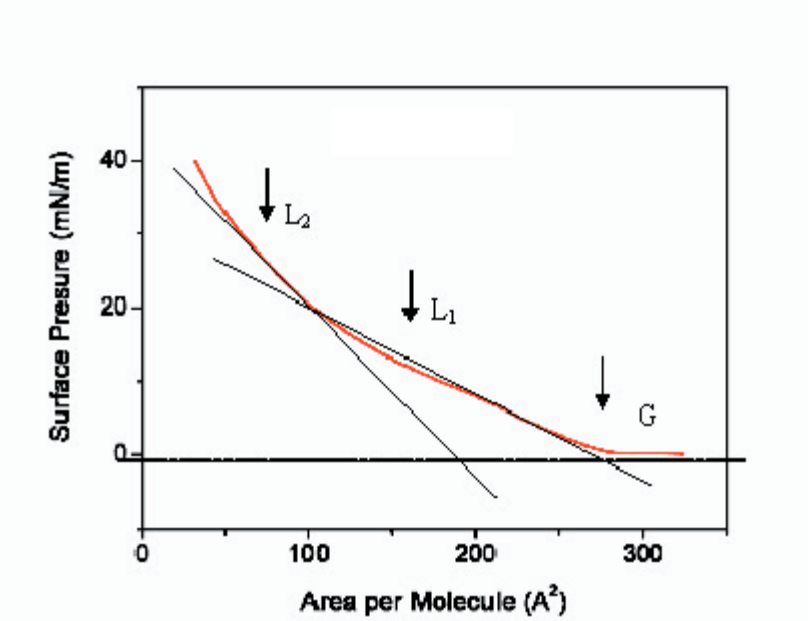

Figure 16: Plot of Surface Pressure Versus Molecular Area for Pure M2 Monolayer. The three distinct phases can be seen. The gas-like phase (G) is present near the onset of pressure at the surface of the air-water interface. This onset area can be estimated using the intersection of the area-per-molecule axis and the tangential slope of the first incline in the curve. The monolayer then changes to a liquid-expanded phase (L_1) and finally to a more compressed liquid phase (L_2). In a similar manner to estimating onset area, the transition areas can also can be determined.

the liquid-condensed phase. From our Brewster Angle Microscopy (BAM) data, as shown in Figure 17, we can clearly see the morphology of the peptide at the different phases as well as a clear collapse of the film at the surface at sufficiently high surface pressures. Qualitatively, the observation can be made that the film is microscopically fluid until it collapses. According to the surface-pressure- area isotherms for different dilutions of the original 0.0625 mg/mL solution of M2 there appears to be a concentration dependence for the phase transitions, as shown in Figure 18. Estimations based on the dimensions of the α-helix formed by the 23 amino acid M2 sequence for the vertical and horizontal areas gives approximately 169 $Å^2$ and 585 $Å^2$ respectively. Comparing this to the areas of onset and limitation for the more concentrated, undiluted sample, we can see that a vertical, close-packed peptide layer is a viable phase organization.

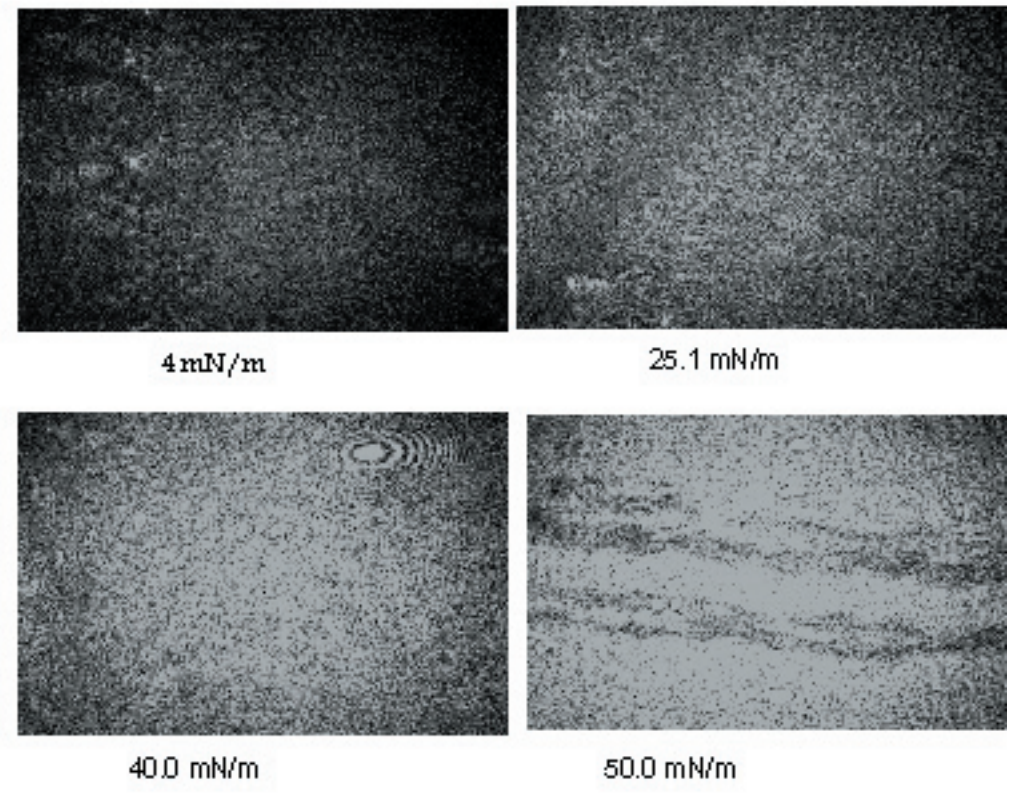

Figure 17: Surface Morphologies of M2 Near Phase Transitions. Images from Brewser Angle Microscopy of pure M2 monolayers show clear phase transitions of the gas-like phase at 4 mN/m, liquid-expanded phase at 25.1 mN/m, and the compressed liquid phase at 40 mN/m. A clear collapse in the membrane evidenced by the large streaks across the surface, can be seen at higher pressures.

However, as the concentration decreases, this organization at the air-water interface becomes less likely. It is also noteworthy that this concentration dependence of the area per molecule for the M2 peptide alone is particularly high (see Table 1). At higher concentrations the film appears to have a reasonable behavior, with reasonable values for the molecular area. As we've already discussed, at higher concentrations the amphipathic helices order themselves at the interface. However, the onset areas for more dilute samples appear much higher than might be predicted. The onset area of 270 $Å^2$ determined for the concentrated sample, agrees well with the estimates of the M2 surface area predicted from the dimensions of the peptide itself. As the samples

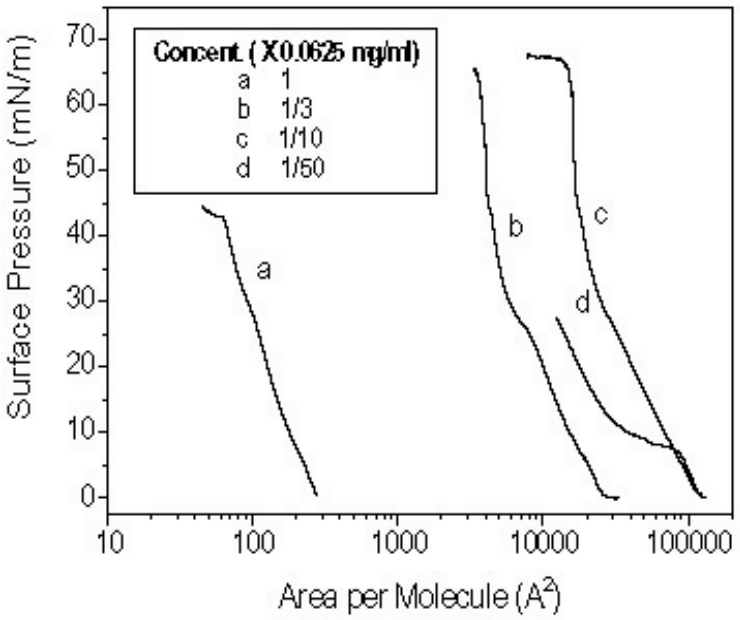

Figure 18: Surface Pressure per Area for Various Dilutions of M2. Here we can see the behavior of the monolayer as the 0.0625 mg/mL sample of M2 is diluted. The more dilute samples appear to have more pronounced transitions and they occur at higher molecular areas.

become more dilute, a possible explanation for the increase in onset area and limitation area is that the M2 peptides no longer form helices, but instead are present

Table 1: Comparison of Onset and Phase Limitation Areas for Different Dilutions of M2. The areas were estimated for the four curves (a-d) from Figure 18. The areas seem to increase greatly upon initial dilution (three degrees of magnitude) but less quickly in subsequent dilutions (one order of magnitude each).

Curve	a	b	c	d
A_{onset} (Å²)	270	27,000	115,000	125,000
A_{lim} (Å²)	140	4,500	18,000	-

at the surface as random coils. Using this model, a packed uncoiled 23 amino acid polypeptide chain is estimated to have a surface area of 1010 Å^2 and a loose-packed configuration at the surface of random-coil M2 peptide would have an estimated surface area of approximately 10^4 Å^2. Looking at the curves the one-third dilution

of the original sample is probably going from an uncoiled, loose-packed phase to a close-packed but still uncoiled phase at higher to surface pressures. What is unclear is what is occurring at further dilutions. The onset area is observed on the order of 10^5 $Å^2$/molecule for these concentrations, which is about an order of magnitude larger than expected based on the dimensions of the M2 molecules. These areas have been confirmed by using compression-decompression-recompression cycles. At such high surface areas, there is very little isobaric creep at low pressures, and the shape of the curve is consistent over many cycles. This indicates that the phase that they are in is at

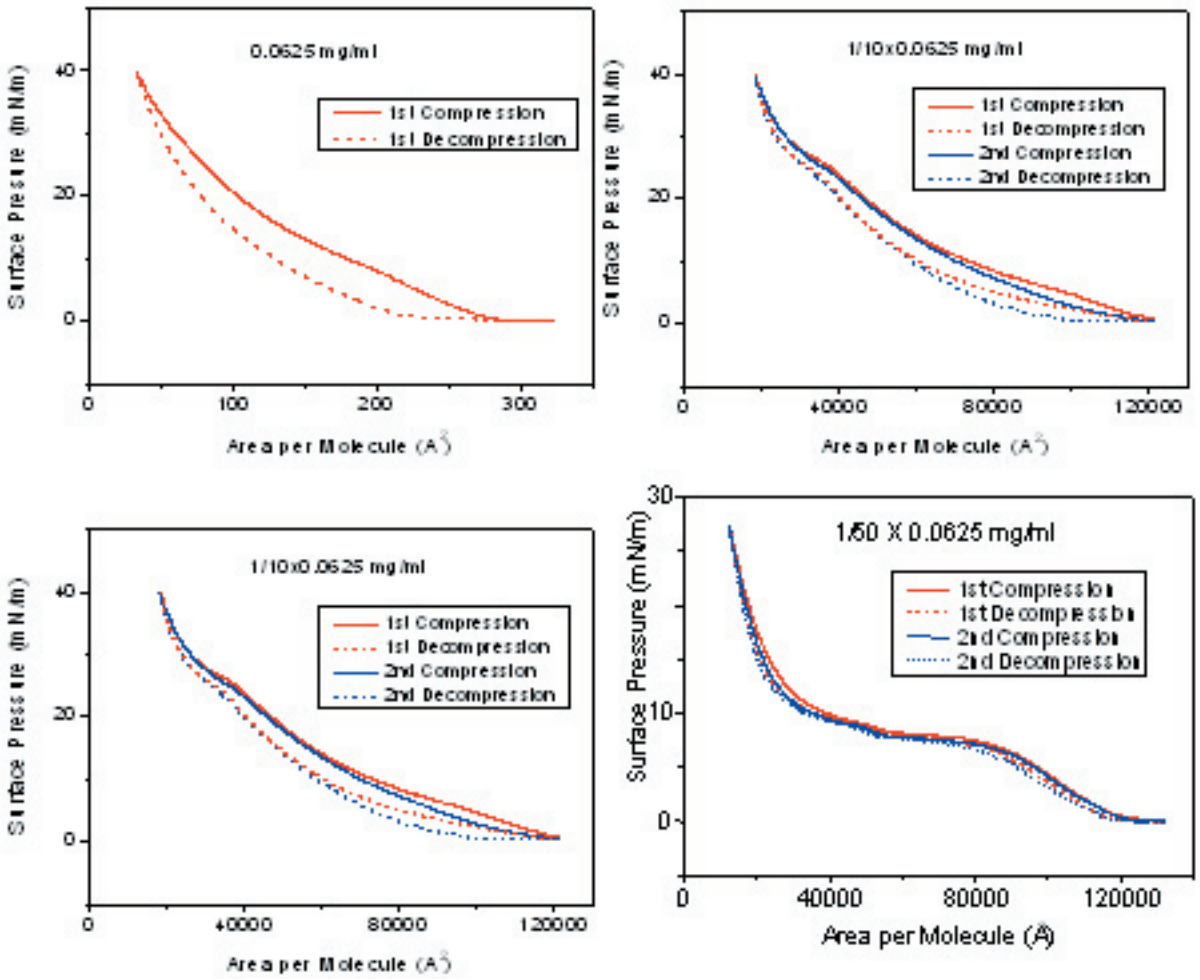

Figure 19: Surface-Pressure Versus Molecular Area Histograms for Different Dilutions of M2. In all cases, after multiple compressions and decompressions, the shapes of the curves are retained. This indicates that the M2 monolayer has reasonable elasticity.

least relatively stable and they maintain good surface elasticity and fluidity (see Figure 19).

Next we wanted to examine the mixing behavior of M2 in DPhPC monolayers. Monolayers formed with pure DPhPC remain in a single phase from onset until collapse with a surface area per molecule of about 100 $Å^2$. As the data shows in Figure 20, for

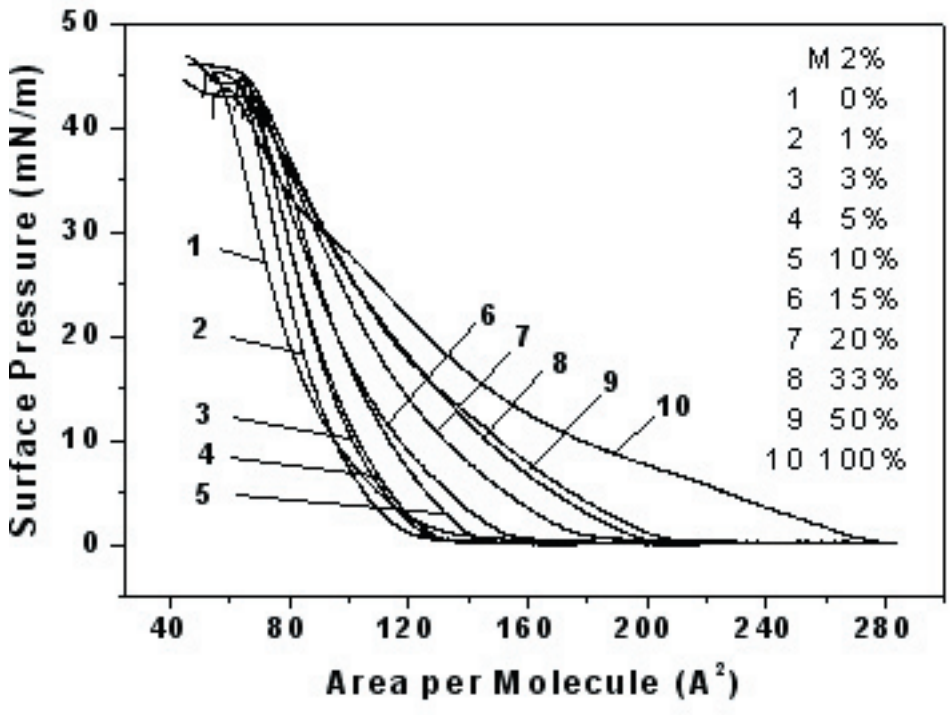

Figure 20: Surface-Pressure versus Molecular Area for Various Mixtures of M2 in DPhPC. Based on the shapes of the isotherms, we can see more pronounced phase-transitions for mixtures that have greater concentrations of M2. Thus for these monolayers the behavior at the surface is dominated by protein properties. Below approximately

lower concentrations (less than 5 mol% M2) it appears that it is the behavior of the lipid that dominate the overall behavior of the monolayer at the air-water interface. This is evidenced by the similarity of the isotherm curves of pure DPhPC and the lower mole fraction of M2 sample. Greater M2 concentrations lead to curves that are more similar to those for pure M2, with three distinct phases, which would indicate that it is the peptide that is determining the behavior for the monolayer at these concentrations. It is possible that the peptides are aggregated in this case, which may act to decrease the close-packing

of the monolayer, and thus, decrease the overall stability. In all cases, regardless of the concentration of M2 present, the monolayer is collapsed at surface pressures of 45± 2 mN/m. It can be seen in Figure 21 by comparing the area per molecule as a function of the mole fraction of M2 at different surface pressures, that there is at least some miscibility

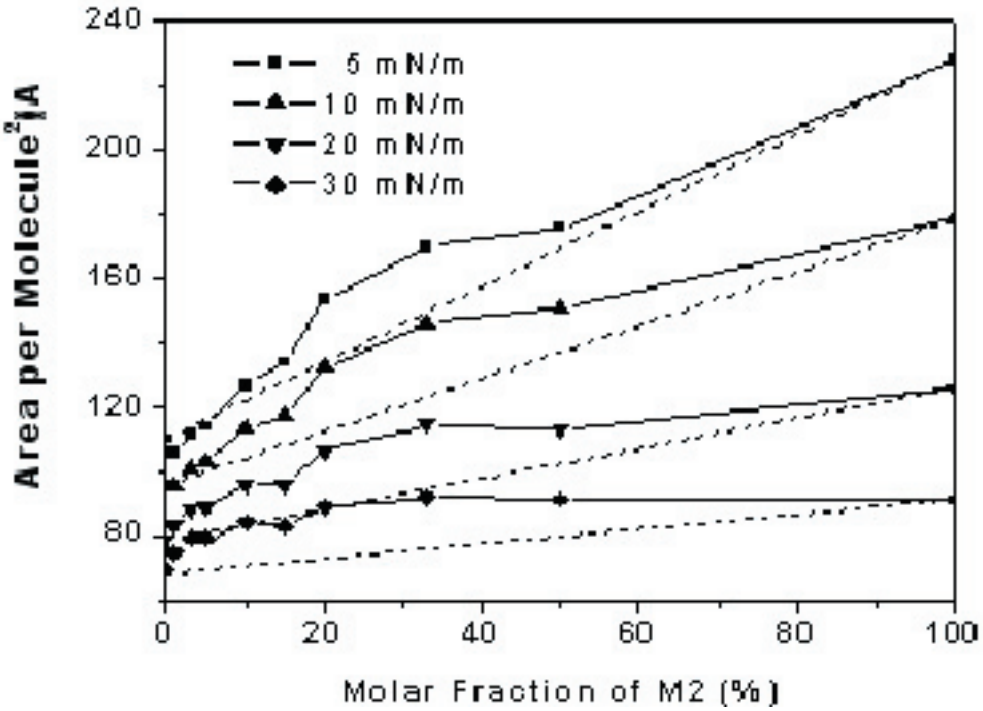

Figure 21: Molecular Area Versus Mole Fraction of M2 at Various Surface Pressures. Based on the comparison of the observed molecular areas to the phase lines at these pressures (dotted lines) indicates at least some miscibility between M2 and DPhPC.

between the peptide and the lipid at the interface.

The electrophysiology of the M2δ channel was studied in different lipid environments, with special attention paid to DPhPC bilayers. Giga-ohm seals were attained consistently with all lipid compositions. The lifetime of these seals could vary significantly; however, seals of pure bilayer (with no channel incorporation) could be maintained for time on the order of hours for DPhPC bilayers (see Appendix for full data sets). We were able to incorporate M2 ion channels into the membrane and demonstrate functionality. The first step was to demonstrate that current flow recordings were actually due to channel function rather than simply being caused by

leaky seals or formation of non-gating oligomer pores by M2. In order to show this a gradient was set up across the membrane formed at the tip of the patch clamp pipette. With no applied voltage across the membrane, the baseline remained flat, as shown in Figure 22. When a voltage was applied, single-channel fluctuations could be seen,

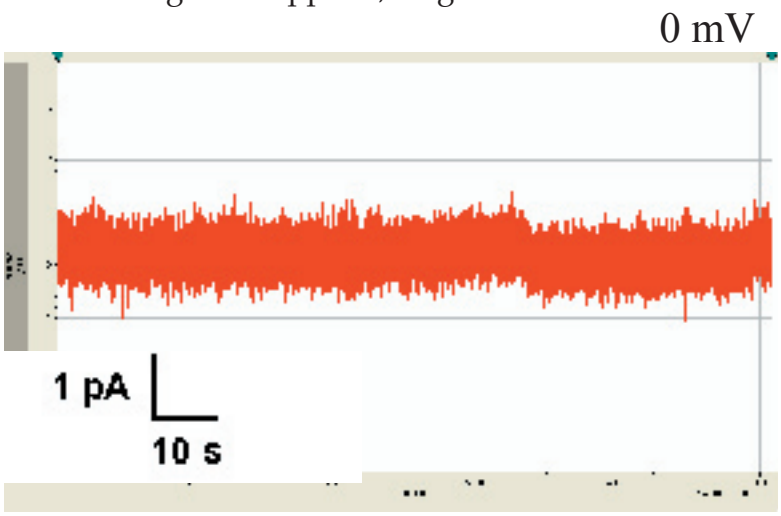

Figure 22: Single-Channel Recording of 1:1000 M2:DPhPC with Ionic Gradient at 0 mV. When no voltage is applied across the membrane, we see no change in the observed current, indicating that

confirming that the pentamer was forming, and functioning as a voltage-gated channel as seen in Figure 23.

Once this was confirmed, we could continue with other electrophysiology experiments. Experiments were carried out with the ion gradient across the membrane

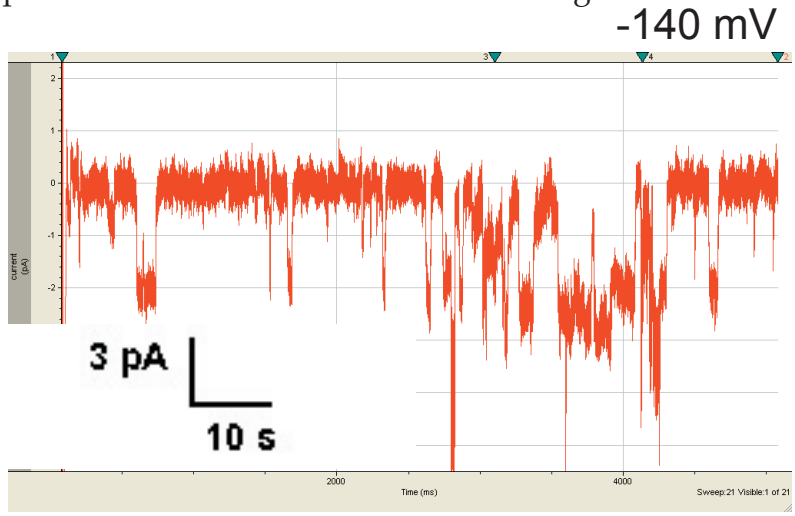

Figure 23: Single-Channel Recording of 1:1000 M2:DPhPC with Ionic Gradient at -140 mV. When a voltage is applied , stochastic current fluctuations are seen, indicating that the M2 peptides have inserted in the bilayer and are functioning as voltage-gated ion channels.

and under isotonic conditions. The figures below demonstrate measurement of channel functions with an ion gradient. When a potential of 0mV was applied across the membrane, no current flow was recorded. Whenever a voltage clamp at -100mV was applied, channel fluctuations were observed, in this case with a mean amplitude of 3 pA. Stochastic channel fluctuations were recorded for each of the different lipid environments described previously, with and without an ionic gradient. Channel fluctuations were recorded for long time scales on the order of minutes to tens of minutes, with continued channel function for the duration of these times as shown in Figure 24. The limiting factor in channel observations on these long time scales was usually the maintenance of the patch at the tip of the pipette. Current flow could usually be seen in

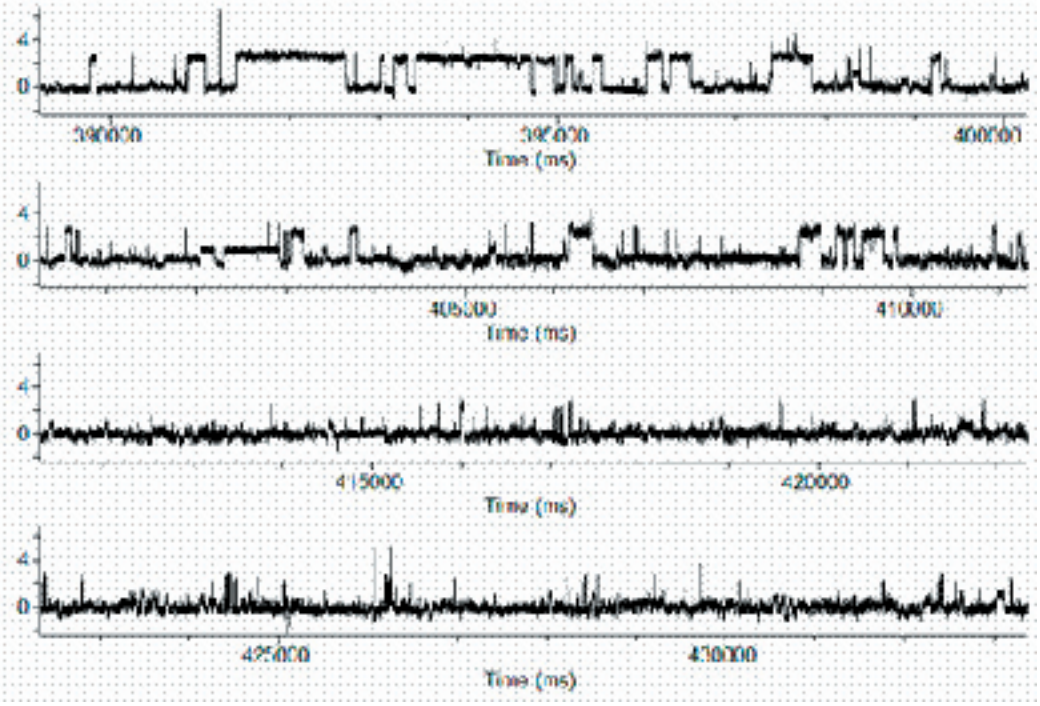

Figure 24: Example of Long-Time Recordings at 100mV. In this 42-second trace, we can see the stochastic opening and closing of the ion channel with a single channel current amplitude of about 3 pA.

these recordings until the gigaohm seal was lost.

There are a few other important results to note. First, the current amplitudes of channels even within the same lipid environment could vary quite significantly. This is particularly true of M2 in DPhPC. First-level currents could be from just below 2 pA to

as much as 8 pA. Thus when mean conductance was calculated to be 23. pS, there was a standard deviation of 13.8 pS. This variation was less pronounced in the native lipid environments, even with the addition of cholesterol.

Also noteworthy is that on occasion, semi-open states could be observed, in which the current amplitude was not as expected for a second ion channel opening simultaneously, but had instead a smaller amplitude near the first level as shown in Figure 25.

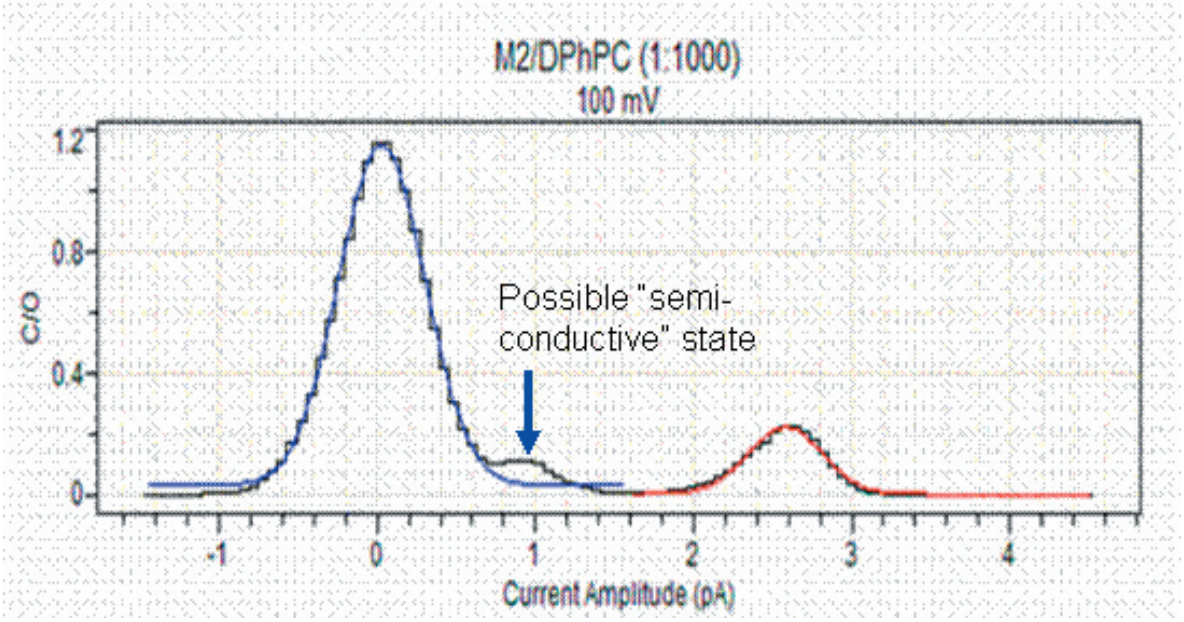

Figure 25: Closed/Open Probabilities for 1:1000 M2:DPhPC Sample at 100mv. The center of the fitted Gaussian function gives the mean-current amplitude of the given state. The relative areas under the curves give the probabilities of finding the channel in either the open or closed state.

For the natural lipid environments the mean conductances were approximately the same regardless of the amount of cholesterol. These conductances range between 19 and 21 pS, with standard deviations between 1.6 and 5 pS. The mean open probabilities also did not seem to differ significantly. However, the mean open times appear to increase as the rigidity of the bilayer increases. The average mean open time in 3:1 POPE:POPC was 5.7 ms at 100mV, which increased steadily to 43.6 ms with the addition of cholesterol up to 30%. At the same applied voltage, the average

mean open time of M2 in DPhPC at 100 mV was 190.3 ms (see Figure 26). As with the conductance measurements, however, the mean open times for M2 vary widely from millisecond to second time scales. It was observed that these longer mean open times where more prevalent in the gap-free experiments compared to the step experiments. It is presumed that the reason for these discrepancies is the comparatively short duration

Table 2: Patch Clamp Results for M2 in Various Bilayer Compositions. The data above for the mean conductance, open probability, and open times was calculated for recordings made a 100 mV. The gating threshold is estimated from multiple step protocol runs.

Bilayer Composition	Number of Samples	Mean Conductance (pS)	Mean Open Probability	Mean Open Time (ms)	Gating Threshold (mV)
3:1 POPE:POPC	4	21.6 ± 5.0	0.0815 ± 0.0673	9.8 ± 13.6	40
3:1 POPE:POPC, 30% cholesterol	4	19.9 ± 1.6	0.4833 ± 0.4072	40.1 ± 24.1	40
DPhPC	9	23.7 ± 13.8	0.3609 ± 0.2723	190.3 ± 271.2	50

of the applied voltage may have only been able to produce opening bursts rather than sustained channel function. These results possibly suggest that while increasing the rigidity of the membrane might not significantly affect the probability of the channel opening, it may hinder random fluctuations of the helices once they are in an open conformation. Thus once open, the channels remain open longer in a more rigid lipid environment.

These results lead to many other issues and experiments that should be performed. The fact that there was much more variation seen in the recordings made

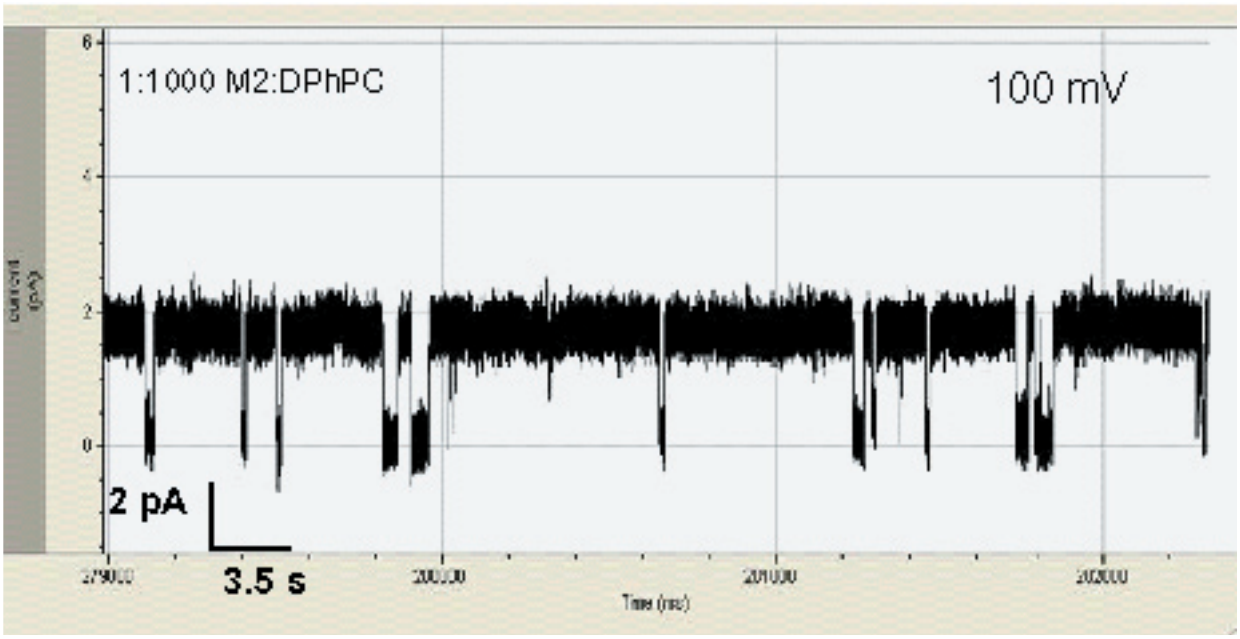

Figure 26: Sample Recording of 1:1000 M2:DPhPC at 100 mV. The average mean open time for M2 in DPhPC is significantly longer than the average mean open time in native lipid combinations.

of M2 in DPhPC than in the other lipid environments may be of some concern for the overall project goal of incorporation into an electronic agonist detection device using tethered phytanoyl moieties. If the variation in the channel function are not systemic and cannot be reduced by other methods, then the M2 channel may not be suitable for detecting micro-quantity differences in agonist concentration. Also, it would be valuable to repeat some of the experiments outlined in this project, particularly electrophysiological measurements for the mixtures of 1:1000 M2 in 3:1 POPE:POPC with the lesser amounts of cholesterol added. There is significantly less data available for these experiments than for those performed in DPhPC, 3:1 POPE:POPC, and the native lipids with 30% cholesterol. Also, experiments with a ramped voltage clamp protocol, using all of the lipid environments outlined here, would be very useful in quantifying the gating differences in M2 as the lipid properties change. The next logical step regarding the electrophysiology of the oliogomeric M2 channels is then to test the

pharmacologic response of the conductance, mean open time, and open probabilities in the presence of agonists, such as anesthetics (Tang and Xu, 2002).

Other future work that should be considered includes obtaining surface-pressure-area isotherms for the native lipids with and without cholesterol. This would allow for a more systematic comparison of the stability of the lipid environment in the presence of M2 peptide. Also, structural studies using solid-state NMR techniques should be considered in order to better understand the dynamics of the channel in these different environments. Such studies may help to explain the observed increase in mean open time as the lipid environment increased in rigidity.

APPENDIX

RAW DATA

The data presented in this appendix are those used for the computation of the values in Table 2 of the text for mean conductance, mean open time, and mean open probabilities for the DPhPC lipid environments (9 total traces). A trace is shown for each of the other lipid environments and more raw data can be obtained upon request. The estimates for the gating voltages were made from data not presented here. In most cases, the data include the filename for each data set as it appears in the compiled database, the recordings after baseline adjustment and filtering at 1 kHz with a Bessel 8-pole filter, and a plot of the open versus closed probabilities for each recording. Note that in some cases there is no open versus closed graph included for particular data sets. This is due to the fact that plots could not be obtained that were consistent with the raw data, however in these cases software calculations that were consistent were obtained and were used in calculations.

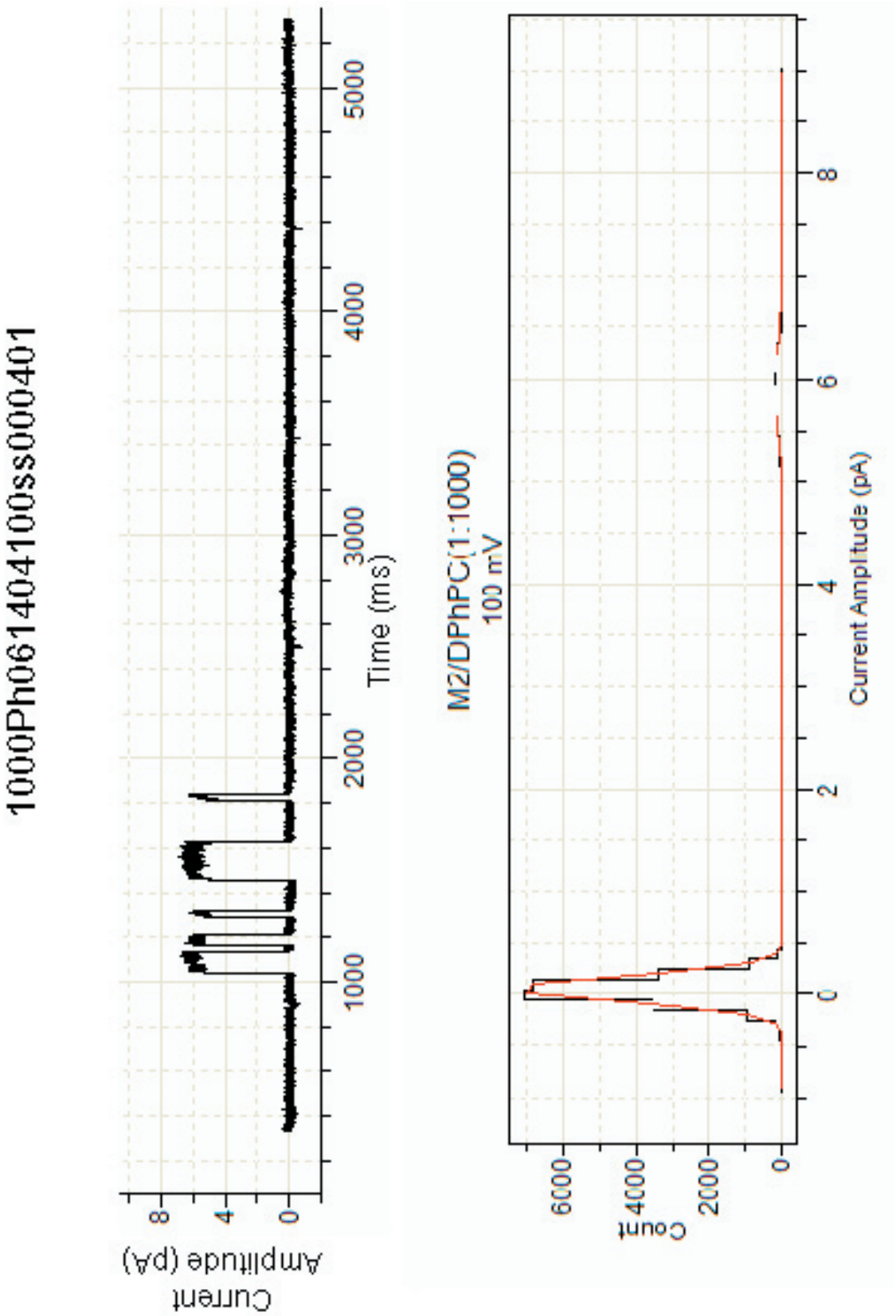
1000Ph061404100ss000401
Current Amplitude (pA)
Time (ms)
M2/DPhPC(1:1000)
100 mV
Count
Current Amplitude (pA)

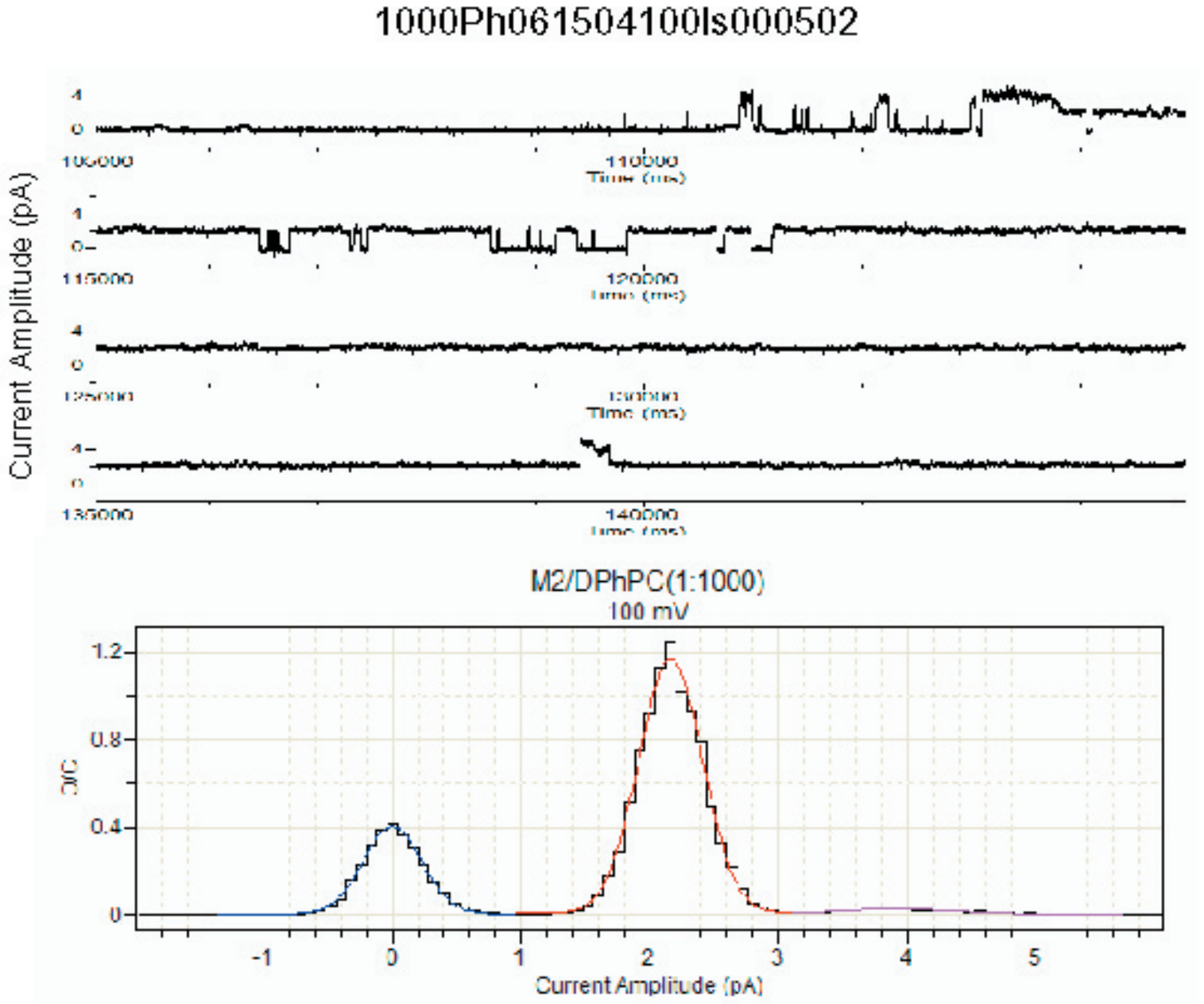
1000Ph061504100ls000502
Current Amplitude (pA)
Time (ms)
M2/DPhPC(1:1000)
100 mV
1.2
0.8
0.4
0
-1
0
1
2
3
4
5
Current Amplitude (pA)

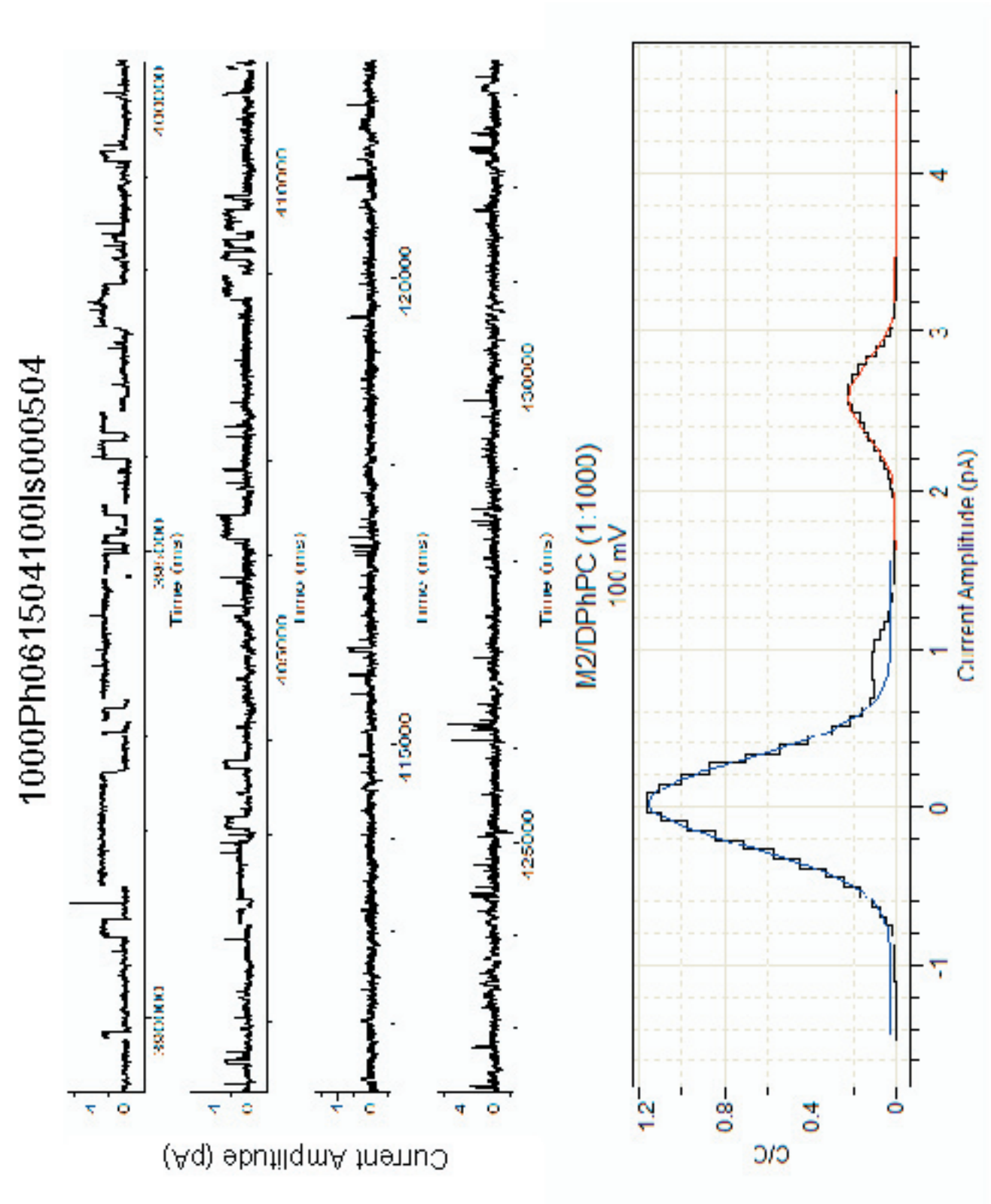
1000Ph06150410011s000504
Current Amplitude (pA)
Time (ms)
M2/DPhPC (1:1000)
100 mV
C/C
Current Amplitude (pA)

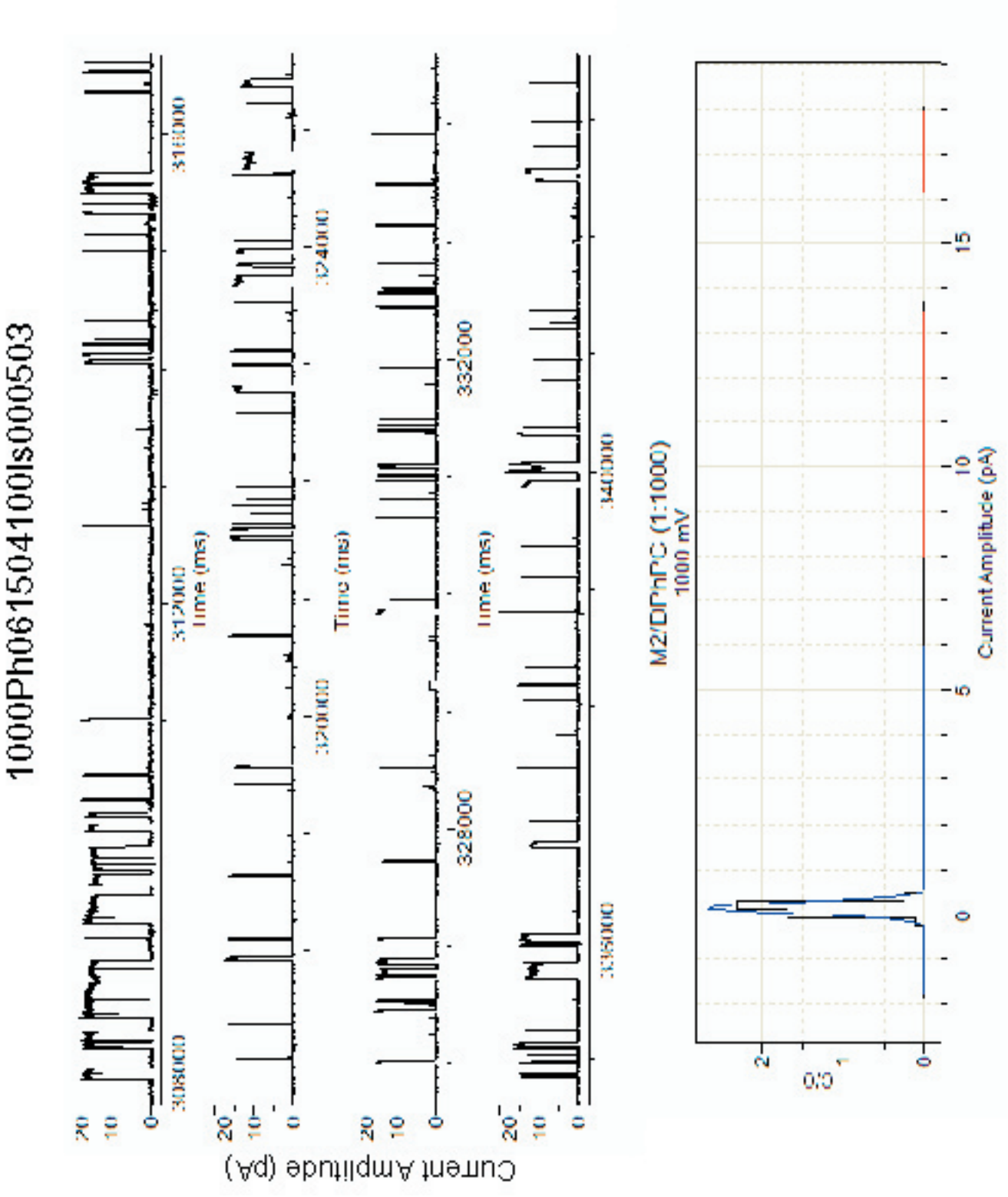
1000Ph06150410Is000503
Current Amplitude (pA)
Time (ms)
M2/DPhPC (1:1000)
1000 mV
Current Amplitude (pA)

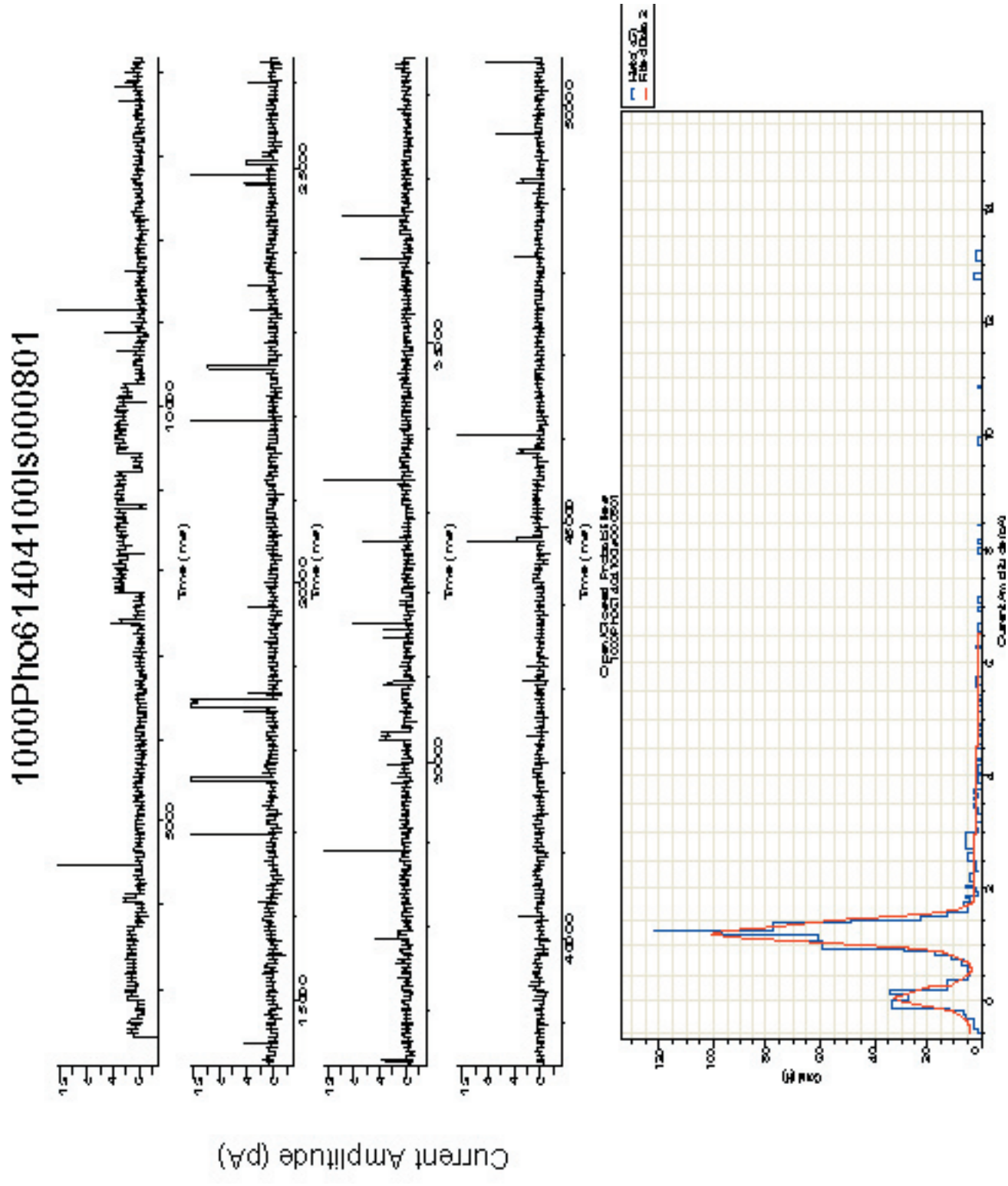
1000Pho6140410Ols000801
Current Amplitude (pA)
Time (ms)
Open/Closed Probabilities
1000Pho6140410Ols000801

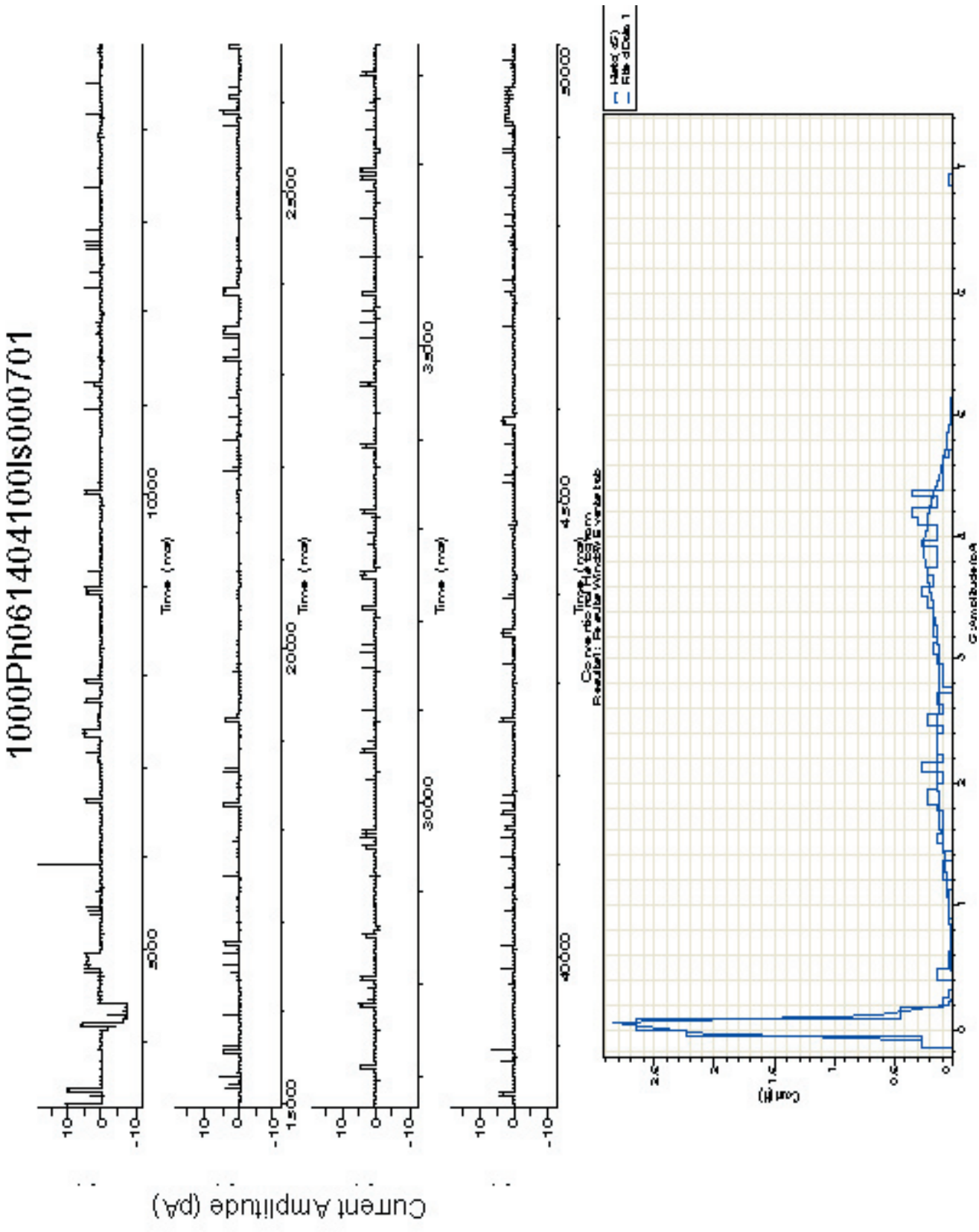
1000Ph06140410001s000701
Current Amplitude (pA)
Time (ms)
5000
10000
15000
20000
25000
30000
35000
40000
45000
50000
Count
Current Amplitude (pA)

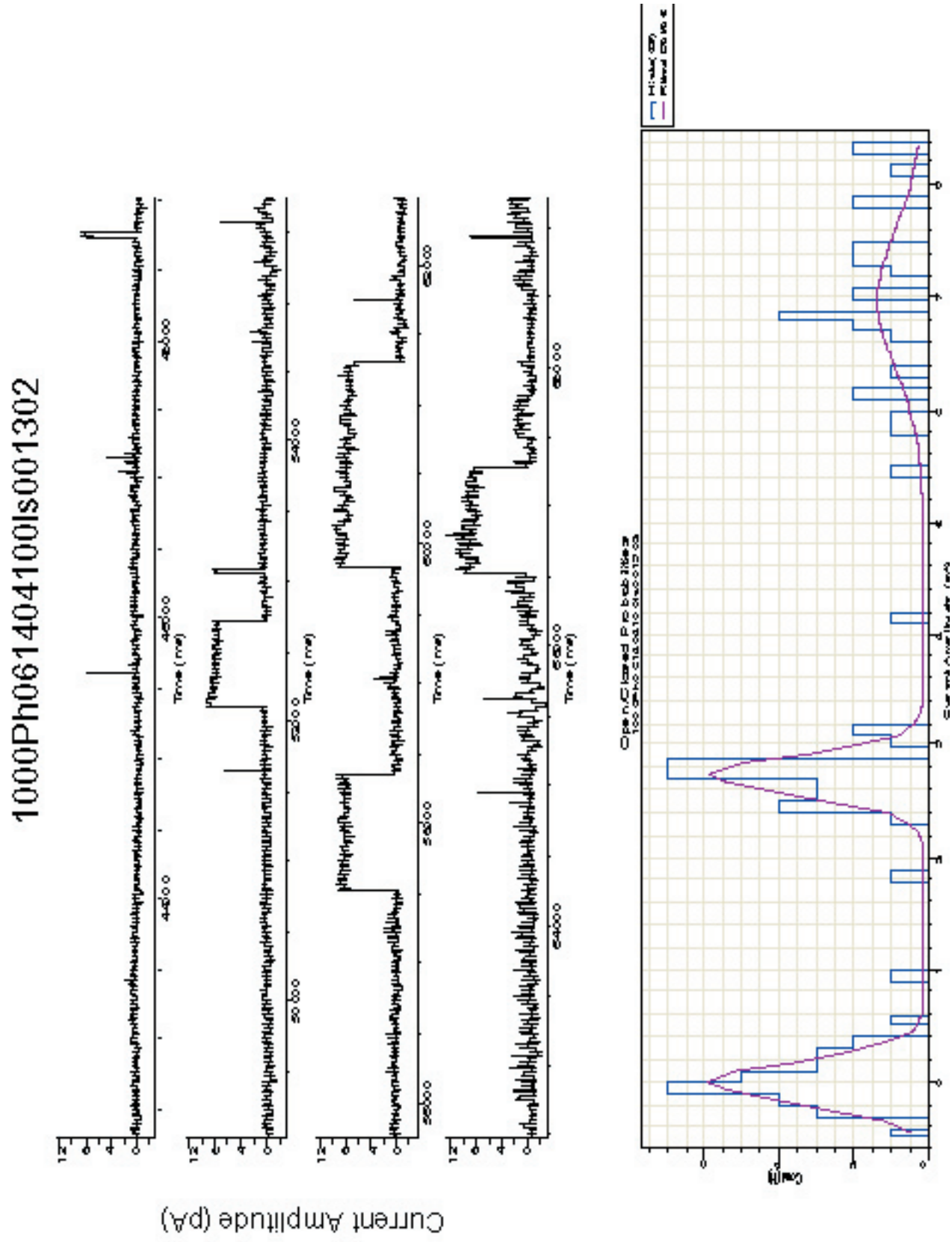
1000Ph06140410Gls001302
Current Amplitude (pA)
Time (ms)

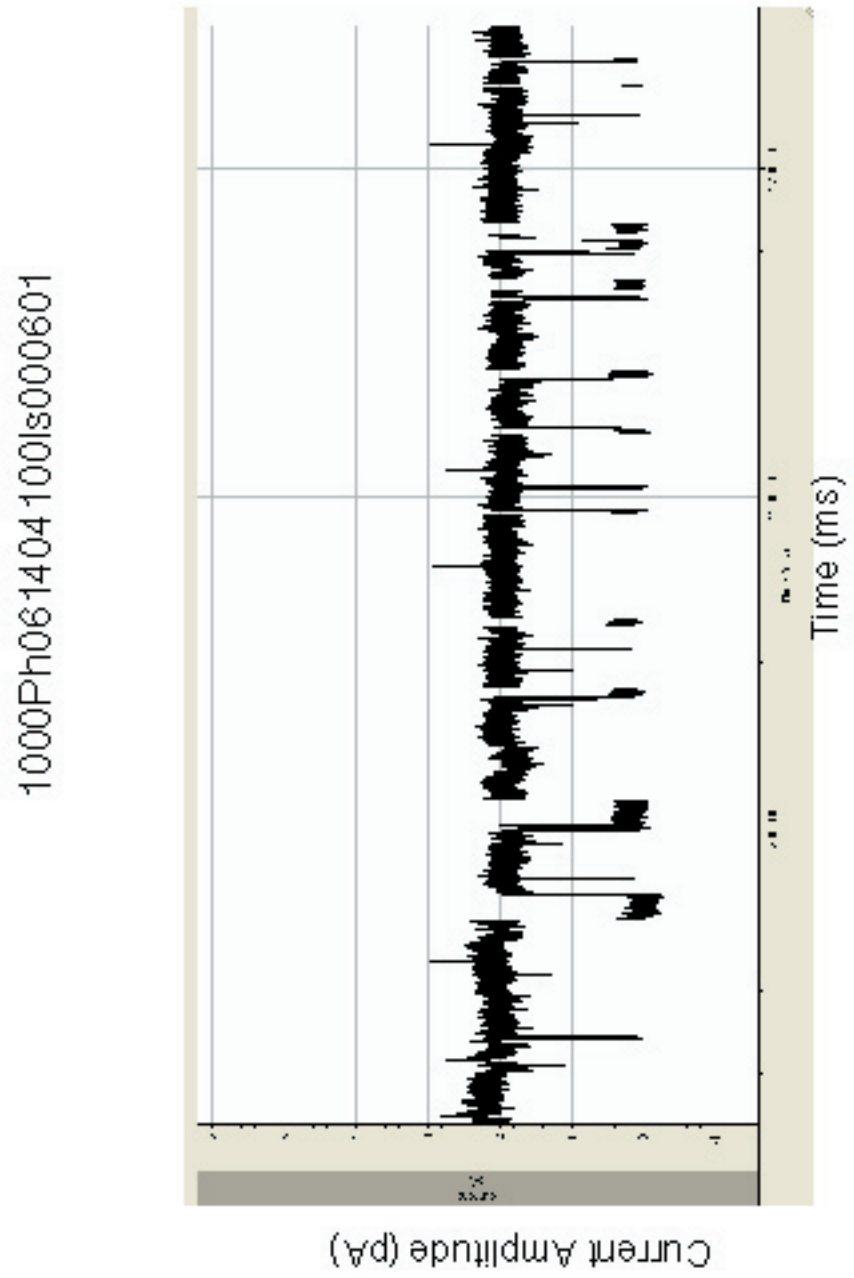
1000Ph061404100ls000601
Current Amplitude (pA)
Time (ms)

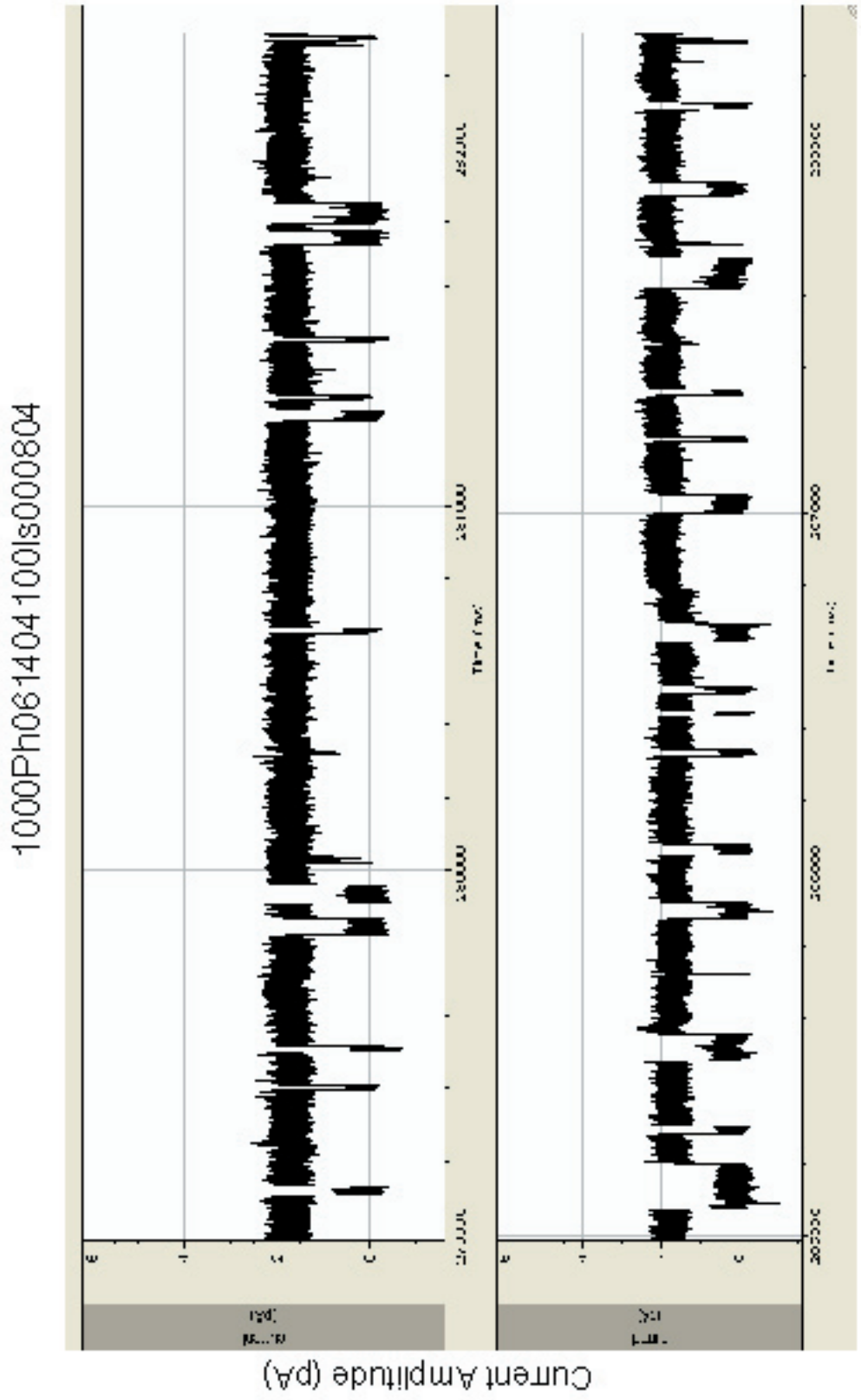
1000Ph061404100ls000804
Current Amplitude (pA)
Time (ms)

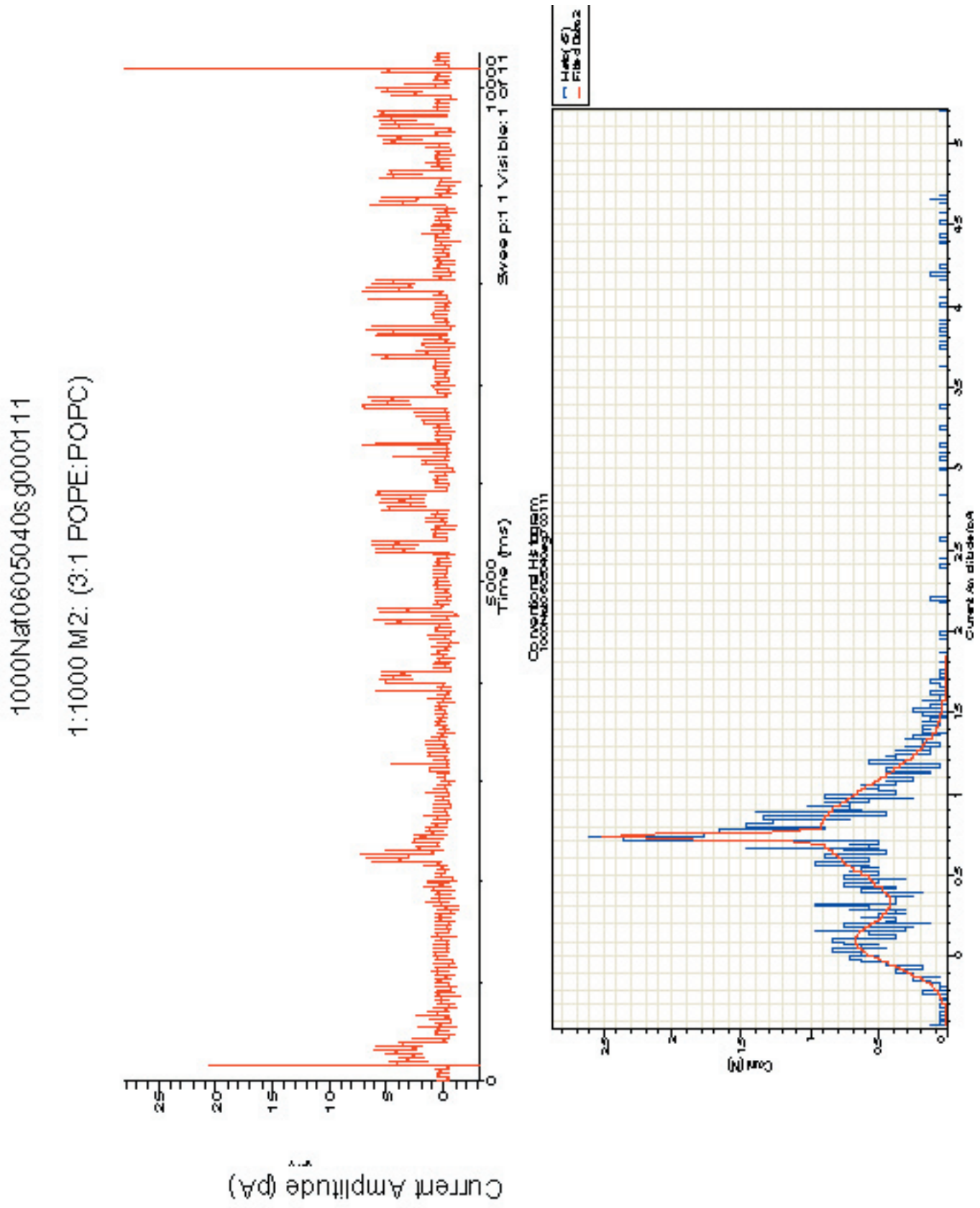
1000Nat060504Osg000111
1:1000 M2: (3:1 POPE:POPC)
Current Amplitude (pA)
Time (ms)
Sweep p:1 1 Visible: 1 of 11
Conventional Histogram
Count (N)
Current Amplitude (pA)

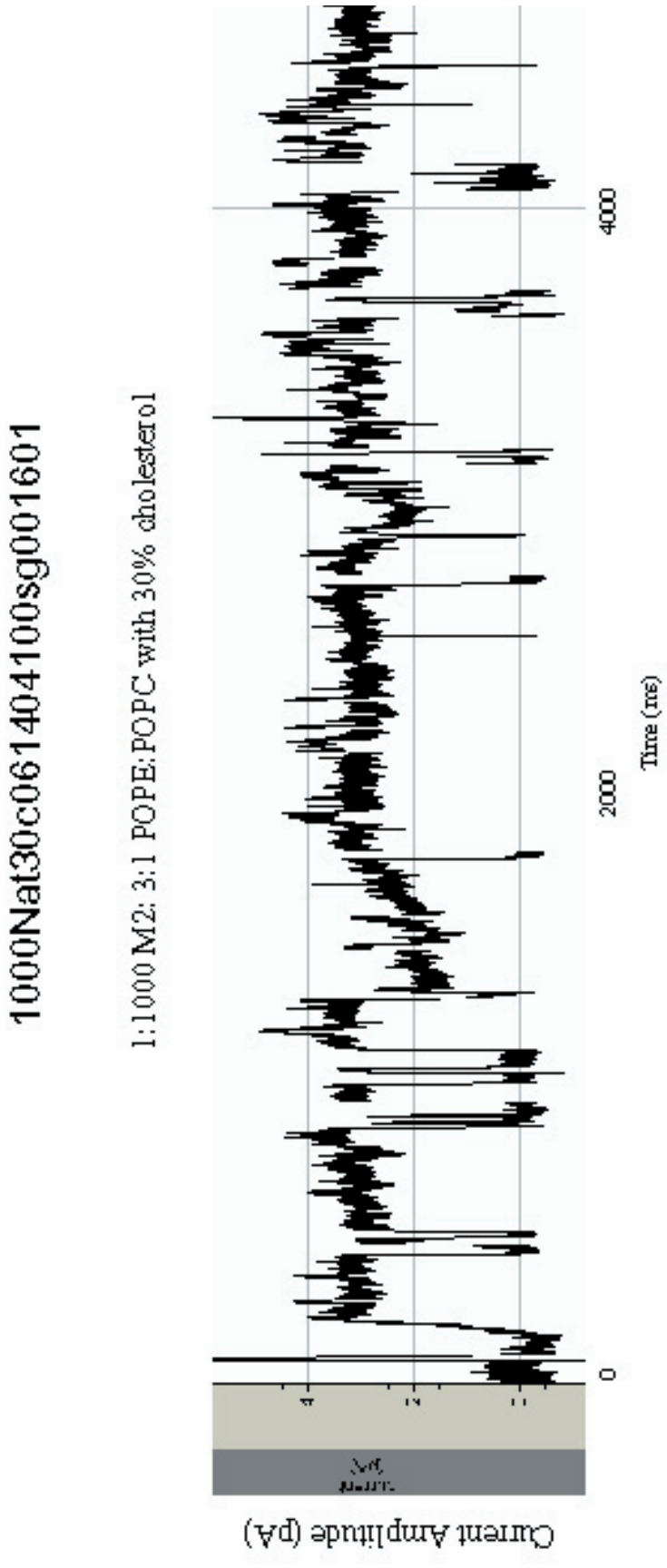
1000Nat30c06140410Osg001601
1:1000 M2: 3:1 POPE:POPC with 30% cholesterol
Current Amplitude (pA)
0
2000
4000
Time (ns)

REFERENCES

Adamson A.W. (1976) *Physical Chemistry of Surfaces*. Wiley & Sons, New York.

Almers W. (1978) *Rev. Physiol. Biochem. Pharmacol.* 82, 96-190.

Binks B.P. (1991) *Adv. Colloid Interface Sci.* 34, 343.

Breed, J., Sankararamakrishnan, R., Kerr, I.D., Sansom, M.S.P. (1996). *Biophysical Journal.* 70: 1643-1661.

Breton M. (1981) *J. Macromol. Sci. – Rev. Macromol. Chem.* C21, 61.

Bringezu F., Dobner B., Brezesinski G. (2002) *Chem. Eur. J.* 8, 3203-3210.

Cantor R.S. (2003) *Am. Chem. Soc.* 42, 11891- 11897.

Carr D. (2002) *The Handbook of Analysis and Purification of Peptides and Proteins by Reversed-Phase HPLC*, 3rd ed. W.R. Grace & Co-Conn, New York.

Chattoraj D.K., Birdi K.S. (1984) *Adsorption and the Gibbs Sruface Excess*. Plenum Press, New York.

Coronado R., Latorre R. (1983) *Biophys. J.* 43, 231-236.

Din L., Li J., Dong S., Wang E. (1996) *J. Electroanalytical Chem.* 416, 105-112.

Gaines G.L. (1966) *Insoluble Monolayers at the Liquid-Gas Interface*. Wiley-Interscience, New York.

Galzi J-L., Devillers-Thiery A., Hussy N., Bertrand S., Changeux J-P., Bertrand D. (1992) *Nature.* 359, 500-505.

Harkins W.D. (1952) *The Physical Chemistry of Surface Films.* Reinhold, New York.

Hoeger C., Galyean R., Boublik J., McClintock R., Rivier J. (1987) *Biochromatography*. 2, 134-142.

Hille B. (2001) I*on Channels of Excitable Membranes*, 3rd ed. Sinauer Associates, Inc, Sunderland, Massachusetts.

Hucho F., Oberthur W., Lottspeich F. (1986) *FEBS Lett*. 205, 137-142

Hucho F., Weise C. (2001) *Angew. Chem. Int.* Ed. 40, 3100-3116.

Imoto C., Busch C., Sakmann B., Mishina M., Konno T., Nakai J., Bujo H., Mori Y., Fukuda K., Numa S. (1988) *Nature (Lond.)* 324, 670-674.

Keleshian A.M., Edeson R.O., Liu G-J., Madsen B.W. (2000) *Biophys. J*. 78, 1-12.

Laughlin R.G. (1994) *The Aqueous Phase Behaviour of Surfactant*. Academic Press Inc., San Diego.

Montal M., Opella S.J. (2002) *Biochimica et Biophysica Acta*. 1565, 287-293.

Nikolelis D.P, Krull U.J. (1993) *Electranalysys*. 5, 539.

Numa S. (1989) *Harvey Lect*. 83, 121-165.

Oblatt-Montal M., Bühler L.K., Iwamoto T., Tomich J.M., Montal M. (1993) J. *Biolog. Chem*. 268, 14601-14607.

Opella S.J., Marassi F.M., Gesell J.J., Valente A.P., Kim Y., Oblatt-Montal M., Montal M. (1999) *Nature America*. 6, 374-379.

Pantola R., Sigg D., Blunck R., Bezanilla F., Heath J.R. (1994) *Biophys. J*. 81, 2389-2394.

Pereira L.G.C., Johansson C., Radke C.J., Blanch H.W. (2003) *Am. Chem. Soc.* 19, 7503-7513.

Petty M.C. (1992) *Thin Solid Films*. 210/211, 417.

Revah F., Bertrand D., Gaizi J-L., Devillers-Thiery A., Mulle C., Hussy N., Bertrand S.,

Ballivet M., Changeux J-P. (1991) *Nature*. *353*, 846-849.

Rivier J., McClintock R., Galyean R, Anderson H. (1984) *J. Chrom*. 288, 303-328.

Roberts G., Ed. (1990) *Langmuir-Blodgett Films*. Plenum Press, New York.

Shaw D.J., (1980) *Introduction to the Colloid and Surface Chemistry*, Butterworth & Co, London.

Suarez-Isla B., Wan K., Lindstrom J., Montal M. (1983) *Biochem*. 22, 2319-2323.

Sunshine C., McNamee M.G. 1992. *Biochim. et Biophys. Acta* 1108, 240–246.

Swalen J.D., Allara D.L., Andrade J.D., Chandross E.A., Garoff S., Israelachvili J., Carthy T.J., Murray R., Pease R.F., Rabolt J.F., Wynne K.J., Yu H. (1987) *Langmuir,* 3, 932.

Tang P., Xu Y. (2002) *Proc. Natl. Acad. Sci*. 99, 16035-16040.

Unwin N. (1995) *Nature*. 373, 37-43.

Vist M.R., Davis J.H. (1990) *Biochem*. 29, 451-464.

Vollhardt D., Gloede J., Weidemann G., Rudert R. (2003) *Am. Chem. Soc.* 19, 4228-4234.

Wagner M.L., Tamm L.K. (2000) *Biophys. J.* 79, 1400-1414.

Yang Y-B., Harrison K., Carr D., Guiochon G. (1992) *J. Chrom*. 590, 35-47.

Yeung C-K., Ingebrandt S., Krause M., Offenhäuser A., Knoll W. (2001) *J. Pharmacol. And Toxicol. Methods*. 45, 207-214.

BIOGRAPHICAL SKETCH

Frank Raucci was born in Pittsburgh, Pennsylvania, in 1981. His family moved to Jupiter-Tequesta, Florida, where he spent the majority of his childhood, in 1984. He attended Suncoast Community High School in Riviera Beach and graduated in 1999 from the Math, Science, and Engineering and International Baccalaureate Magnet Programs. His formal, post-secondary education began at the University of Florida in the Fall term of 1999. While participating in undergraduate research projects throughout his time at the University, he graduated magna cum laude in 2003 with a Bachelor of Arts degree in physics and a Bachelor of Science degree in chemical engineering. He then began work on this project as a requirement for his Master of Science degree in biomedical engineering. Frank will be attending the Medical College of Virginia at Virginia Commonwealth University in Richmond. He will be participating in the MD/PhD program at this institution.